Machine learning-based model of surface tension of liquid metals: a step in designing multicomponent alloys for additive manufacturing

Mariam Assi, Julien Favre, Anna Fraczkiewicz, Franck Tancret

Machine learning-based model of surface tension of liquid metals: a step in designing multicomponent alloys for additive manufacturing

Mariam ASSI[1*], Julien FAVRE[1], Anna FRACZKIEWICZ[1*] and Franck TANCRET[2]

1: Mines Saint-Etienne, Univ Lyon, CNRS, UMR 5307 LGF, Centre SMS, F - 42023, Saint-Etienne, France

2 : Nantes Université, CNRS, Institut des Matériaux de Nantes Jean Rouxel (IMN), 44000 Nantes, France

Abstract: The surface tension (ST) of metallic alloys is a key property in many processing techniques. Notably, the ST value of liquid metals is crucial in additive manufacturing processes as it has a direct effect on the stability of the melt pool. Although several theoretical models have been proposed to describe the ST, mainly in binary systems, both experimental studies and existing theoretical models focus on simple systems. This study presents a machine learning model based on Gaussian process regression to predict the surface tension of multi-component metallic systems. The model is built and tested on available experimental data from literature. It is shown that the model accurately predicts the ST value of binaries and ternaries with high precision, and that identifying certain trends in the ST values as a function of alloy composition is possible. The ability of the model to extrapolate to higher-order systems, especially novel concentrated alloys (high entropy alloys, HEA), is discussed.

Keywords: surface tension, liquid metal, machine learning, data science, Gaussian Process Regression, high entropy alloys, stainless steels

*Corresponding authors: Mariam-assi@hotmail.com, anna.fraczkiewicz@emse.fr

1. Introduction

In recent years, the development of innovatory processes like Additive Manufacturing (AM) has open new possibilities in modern metallurgy. However, the available set of conventional alloys currently known to be reliably processable by AM remains quite limited, and there exist very few materials that are optimized for these processes [1]. Designing new, "AM-dedicated alloys" is challenging [2]–[6]: in such materials, minimization of the defects in final products (like hot cracking, porosity, surface roughness, balling, residual stresses and distortions) is expected. AM processes involve liquid metal, so different properties of materials in this state are of practical importance and need to be studied. Among them, the surface tension (ST) is crucial, as two different effects involving this characteristics may be feared: (i) the ST value influences the conditions of wetting of the previously deposited solid phase by the liquid one; (ii) the absolute ST value and its variation with temperature contributes to the control of the melt pool stability and shape [7].

It is currently admitted that the ST value depends on the temperature of the liquid, pressure and chemical composition of the alloy [8], [9]. Generally, for a wide range of materials, the ST decreases with temperature [10]–[13]. There is no general rule about alloying effects on ST in comparison to pure elements. Typical values in metals and alloys range from $0.4\ N.m^{-1}$ (e.g. Li at 453 K) to $2.5\ N.m^{-1}$ (e.g. W at 3650 K) [9].

Experimental measurement of surface tension in metallic alloys faces many challenges and is subjected to numerous sources of error. The difficulties come from several features. First, the measurements need to be performed in the liquid state, at high temperatures, facing an obvious and difficult to avoid risk of contamination (oxidation). Moreover, real alloys currently contain impurities; some of them (S, O) have a significant effect on ST, decreasing its value even for very

low content in the alloy [14]–[18]. Several methods of experimental assessment of surface tension exist; their details have been reviewed [19]. The Sessile Drop Method (SD), and the pendant drop method (PD) similarly present the advantage of providing values of ST over wide ranges of temperatures [20]; however, the use of reference surfaces and/or capillary tubes respectively is a source of significant error [19]. Surface contamination effects are much less pronounced in the Maximum Bubble Pressure Method (MBPM) in which consecutive measurements are done on a freshly formed surface [21], [22]. Finally, the Electromagnetic Levitation (EL) method provides an enhanced accuracy as it eliminates persistent sources of contamination as mentioned above [19].

Theoretical description of surface tension, based on alloys thermodynamics, started at the beginning of 20^{th} century, with the first approaches proposed by Gibbs [23] and improved by Guggenheim [24], [25]. Finally, the Butler model proposed in 1932 [26] became the most known and used model to estimate the ST values from the chemical composition of the alloy.Although it provides a fair estimation, the Butler model remains inaccurate in many cases, probably due to neglecting the atomic structure of liquid alloy surfaces [19]. Recently, Vermot des Roches *et al.* [27] have compared the results of ST calculations by Butler model to available experimental data on binary alloys : it was shown that the Butler model fails to accurately predict almost 40% of them.

In an attempt to alleviate some of the limitations of the Butler model, Wynblatt et al. [28] presented an approach that is built on the same assumption of the equality of chemical potentials between surface and bulk but instead of a monolayer, the surface was considered to be made of multilayers. Although more general, this model could not really improve the prediction of certain systems such as the Al-Ni system. Egry et al. [29], [30] proposed an analytical model extended from the ideal

solution approach. It was able to significantly enhance the predictions of several systems, for example the Al-Ni and Fe-Ni systems. Yet, a general model that would be able to describe all the existing alloys is still missing.

Some authors proposed models relating the ST value in a given metallic matrix to the presence of different surface-active elements. An interesting approach was presented by Ghebiri *et al.* who proposed a semi-empirical model describing the oxygen content effect in different metallic liquids [31].

Although several theoretical models have been proposed to describe the ST, mainly in binary systems [24], [26], [28], [32], [33], and some authors have used them to estimate the ST values and evolution for ternaries and multi-element alloys [34]–[36], both experimental studies and existing theoretical models focus on simple systems. Rare are the results coming from alloys containing three or more elements, except experimental measurements in several grades of industrial alloys like austenitic stainless steels [37]–[39] and Ni-based superalloys [40], [41]. Besides, the lack of models for multicomponent systems is due to the difficulty in physical modeling the complicated behavior of ST, when several elements are included and the large number of parameters is required to assess.

In this work, a general machine learning-based (ML) model is proposed to predict the surface tension of metallic alloys. The model is based on a Bayesian algorithm, specifically Gaussian Process Regression (GPR). The ambition of the ML-GPR model is to enlarge its application field to multicomponent alloys. Thus, after its training and validation on existing experimental data, the ability of the model to predict surface tension in more complex compositions (like classical stainless steels) and some innovatory concentrated alloys (austenitic single phase HEA alloys from the CoCrFeMnNi family) will be tested.

2. Methods

2.1 Data Processing

The data used to build, train and develop the model come from existing bibliography. Its exhaustive list is referenced and the list of exploited systems is given in Table 4. A large panel of metallic systems (pure metals, binaries, ternaries as well as some multicomponent systems like industrial alloy grades) have been taken into account, in the limits of our best knowledge. All measurement techniques were considered. However, ST data for alloys containing elements such as Na, K, Rb, Cs, Bi and Pb were not considered. In most of the cases, these elements were studied as additives [42] and their low content does not permit a comprehensive extrapolation.

In total, around 2200 data points were collected from approximately 70 scientific articles. The data considered consists of purely experimental data. The elements considered are: Ag, Al, Au, C, Co, Cr, Cu, Fe, Ge, Li, Mg, Mn, Mo, Nb, Ni, Si, Sn, Ta, Ti, W, Zn, and Zr. The data points are measurements recorded at different temperatures, for which around 520 points are for pure elements, 1257 for binary systems, 350 for ternary systems, and less than 140 points for quaternary and higher order systems. Impurities such as oxygen, sulfur and phosphorus, as mentioned in section 1, behave differently and require a different approach. Moreover, in most cases the content of these elements is not specified but rather approximated. Hence, they were not included in the composition vector.

Within the considered alloys and alloying elements, the construction of the database highly depended on the availability of measurements in literature, so that not all elements or materials are represented evenly. This will be discussed later. In addition to the amount of data, another issue lies in the measured values themselves. Each measurement is subjected to an error, whether

experimental or due to the purity of the material studied, both which could vary between different sources. Therefore, a discrepancy in the values is inevitable. For example, Fig. 1 a) shows different values of ST for pure zirconium as reported by different authors and compared by Paradis et al. [43]. The discrepancy in the measurements reaches up to around 0.15 $N.m^{-1}$ at the melting temperature. The authors also showed similar comparisons for pure niobium and pure titanium. Similarly, measurements of ST for pure Fe could vary significantly between different sources. Monma et al. [44] reported a value of around 1.65 $N.m^{-1}$ for pure Fe at 1823 K, while a value of around 1.9 $N.m^{-1}$ was reported by Brillo et al. [45]. Likewise, two sets of values for the Fe-Ti system are shown in Fig. 1b, which will be discussed later. Such scatter in data may largely originate in differences between the various measurement methods mentioned in the introduction. However, in our study all the sets of different values were used, assuming that the statistical nature of the used ML tool (GPR) will allow to smooth out the scatter and extract correct trends. Such an ability was for instance illustrated by the learning of phase formation in multicomponent alloys, from highly scattered data, with large differences coming from a wide diversity of experimental conditions and methods [46]. The resulting model was then trusted, and successfully used for alloy design [47], demonstrating its ability to learn relevant trends from highly noisy data. It was thus chosen here to use all available data (i.e. both old and recent, coming from different measurement techniques). Indeed, on one hand there would not have been a systematic and rational way of deciding what data are good or wrong or better than others, and on the other hand removing all the data appearing scattered would have led to an extremely limited applicability of the model (number of elements, concentration spans).

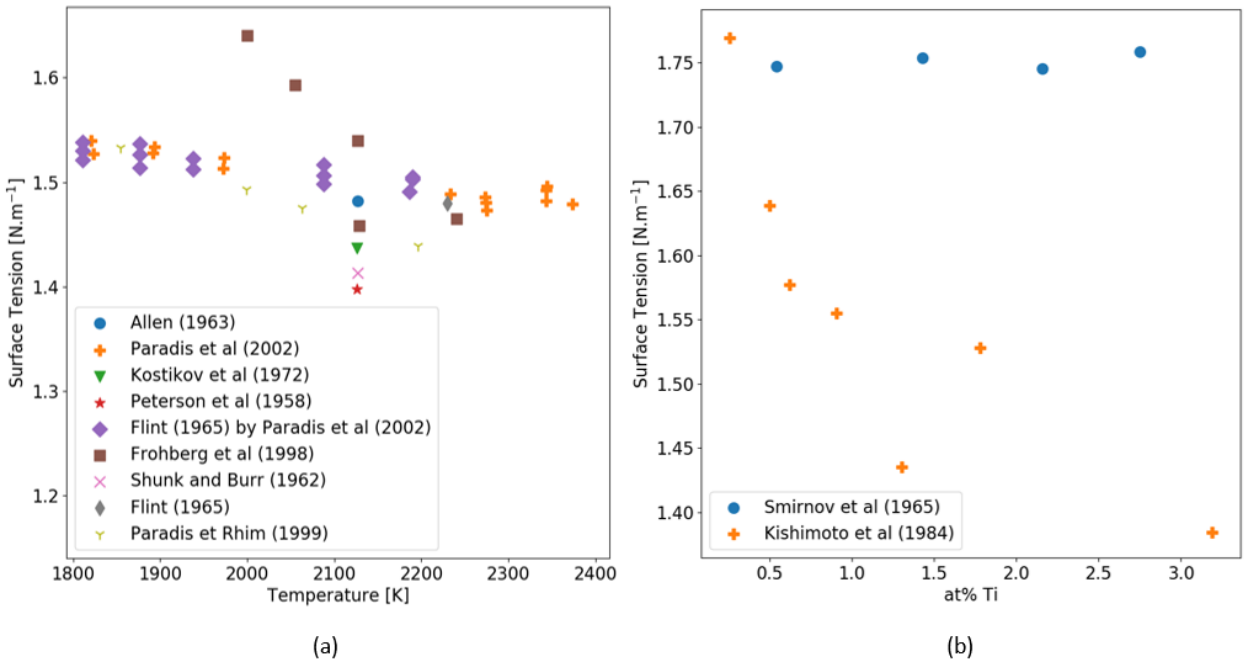

Figure 1 Examples of surface tension data discrepancy for a) pure Zirconium at different temperatures [43],b) Fe-Ti at 1823 K [73] (As cited by [27]), [74])

2.2 Machine Learning Model

Machine Learning (ML) algorithms currently serve as an excellent exploitation tool for available experimental data in the field of materials science [47]–[53]. Although the earliest use of informatics in materials science goes back to the integration of thermodynamic databases into thermochemical computations to map phase stability in binary and ternary alloys [48], with the advancement of the computing power and the different ML algorithms, the use of ML in materials science became more present.

In this study, the proposed model is based on Gaussian Processes Regression (GPR), a Bayesian algorithm that has been successfully used to solve nonlinear prediction problems. Bailer-Jones et al. [54] were among the first to utilize this method in the domain of metallurgy, where they presented a Gaussian Process model for the empirical modelling of austenite formation during the

continuous heating of steels. More recently, this method has been used by several authors to predict material properties [46], [55], [56].

GPR mainly defines a distribution over functions such that for every two or more points chosen, the output of these points follows a joint multivariate Gaussian distribution [57]. A more detailed explanation of the model can be found in Appendix 2. One of the main advantages of using the ML-GPR method is that in addition to predicting a mean value, it also provides a variance for the predicted distribution. In this study, GPR available in the open-source Python package Scikit-learn was used [58].

What is referred to as Gaussian process training is usually the selection of a covariance function (kernel) and its parameters. For this model, the RBF (Radial Basis Function, also known as squared-exponential) kernel was chosen and the lengthscale values were optimized through fitting. The final lengthscales could be insightful as they can provide information on the influence of the input parameters. Usually, the lower the value of the lengthscale, the higher can be the influence of the respective feature, whereas large lengthscales would prohibit steep variations. Lengthscales are optimized such that the model remains smooth and any over-complexity is avoided. This is ensured by the addition of a hyper-parameter indicating the noise level. To ensure that the selection is optimal, a GridSearch technique was applied and repeated for different parameter intervals.

The predictability and the ability of generalization of the ML-GPR algorithm is evaluated by cross-validation to avoid overfitting. The evaluation metrics considered are the most commonly used values for regression and numerical problems, i.e: the Mean Squared Error and Root Mean Squared Error (MSE and RMSE, respectively), Mean Absolute Error (MAE) and R-squared (R^2).

The model hyper-parameters are adjusted to obtain a large R^2, a small MSE and a small RMSE. The variation of these metrics for the different cross-validation folds is discussed hereafter.

3. Results and discussion

3.1. Building the model

The model was first trained and fit on all collected experimental data. The average values of the evaluation metrics for both the training and the testing sets computed with the 10-fold cross-validation method are shown in Table 1. It can be seen that the overall performance of the model is very good with an MSE average of around 0.02 and an R^2 value of 0.97. Fig. 2 shows the cross-validation prediction results as well as the final prediction results of the model after training as a function of the real measurements. The majority of the points lie on the line with slope 1 indicating a generally high prediction accuracy. Nevertheless, there remains a few data points at which the model shows a relatively high error in prediction, especially in the cross-validation test results. Several of these points can be explained by the insufficiency of data to well describe a particular material. For example, Mg and W-based alloys are only described with 14 data points each. Hence, it is unavoidable that the model fails to correctly predict these points when they lie within the testing set. The same could be said about Li and Zn, which are represented with 10 and 24 points respectively, especially that these points are located on the extremes of the database. Li and Mg have some of the lowest ST values of 0.39 and 0.55 $N.m^{-1}$ respectively at their melting temperatures, compared to 3 $N.m^{-1}$ for W. It is also normal to observe that the predicted value for the mentioned points is correct when the model is trained on the whole dataset, as shown in Fig. 2 b. Of course, due to data discrepancy discussed in section 3, there remain a few points that still show a higher error even after training.

	test R^2	train R^2	test MSE	train MSE	test MAE	train MAE
Average	0.9783	0.9950	0.0237	0.0050	0.0581	0.0419
Standard deviation	0.0294	0.0003	0.0369	0.0003	0.0091	0.0008

Table 1 Average and standard deviation values for different evaluation metrics using the 10-fold cross validation method

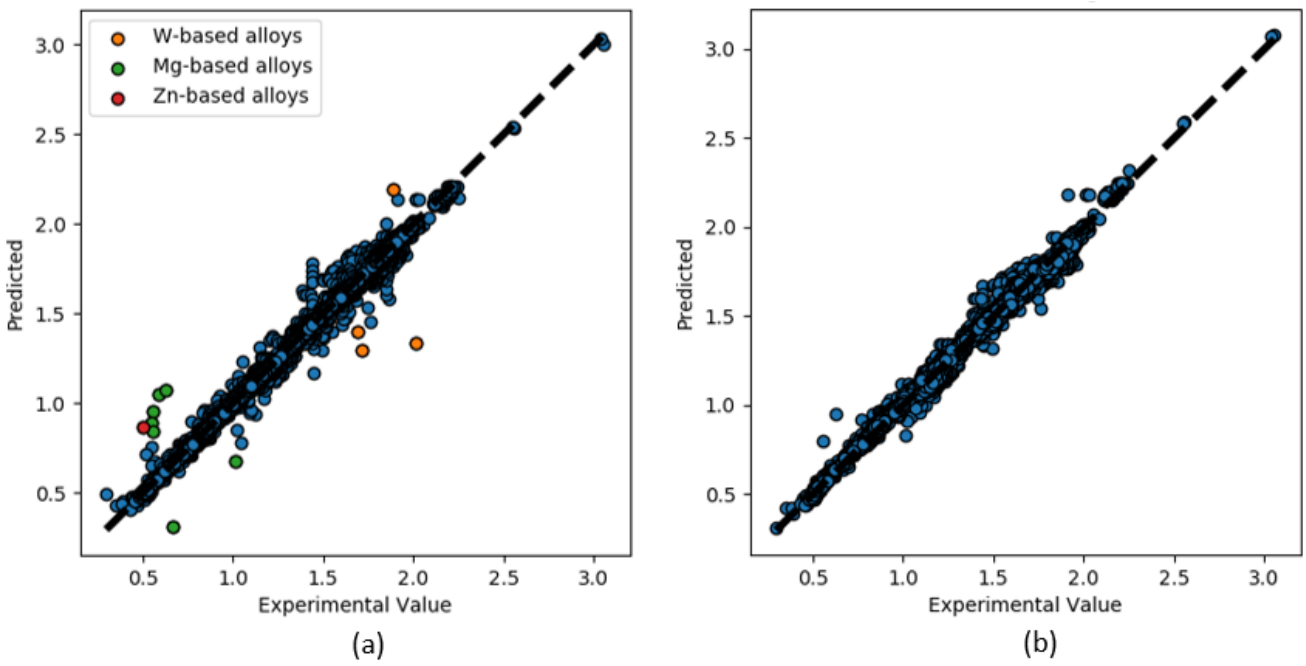

Figure 2 Predicted surface tension values in [$N.m^{-1}$] as function of the experimental values from literature for a) 10-fold cross validation b) the final trained model on the whole dataset

3.2 Model validation: surface tension in binary systems; comparison between experimental values and ML-GPR model prediction

Based on the so built and trained model, the evaluation of surface tension in selected binary systems has been performed. The obtained results have been systematically compared with existing data. Only a few examples of studied systems will be presented and commented on in this paragraph. A complete set of data, for about 20 different binaries, mainly Fe-, Al- and Ni-based, is presented in Appendix 1.

For well-documented binary alloys, the ML-GPR model of surface tension shows its ability to correctly reproduce the trends in ST in binary alloys, as a function of the content of elements. This is the case of Fe-based alloys in which the ST is quite independent of alloying element content (ex: Fe-Cr at 2073 K, Fe-Ni at 1773 K, Fe-Co at 1823 K), as shown in Fig. 3, but also in the case where the addition of an alloying element changes the ST value, as seen in the Fe-Al system at 1233 K (Fig. 3 d).

Also, Al-based alloys are generally well described, as shown in examples in Fig. 4. Let us note that in these materials, any alloying increases the ST value, as the surface tension for pure aluminum is low, of about 0.9 $N.m^{-1}$, and slightly decreasing with temperature. In all these systems, the accuracy of prediction is quite satisfactory, with the 95% confidence interval currently below 0.2 $N.m^{-1}$.

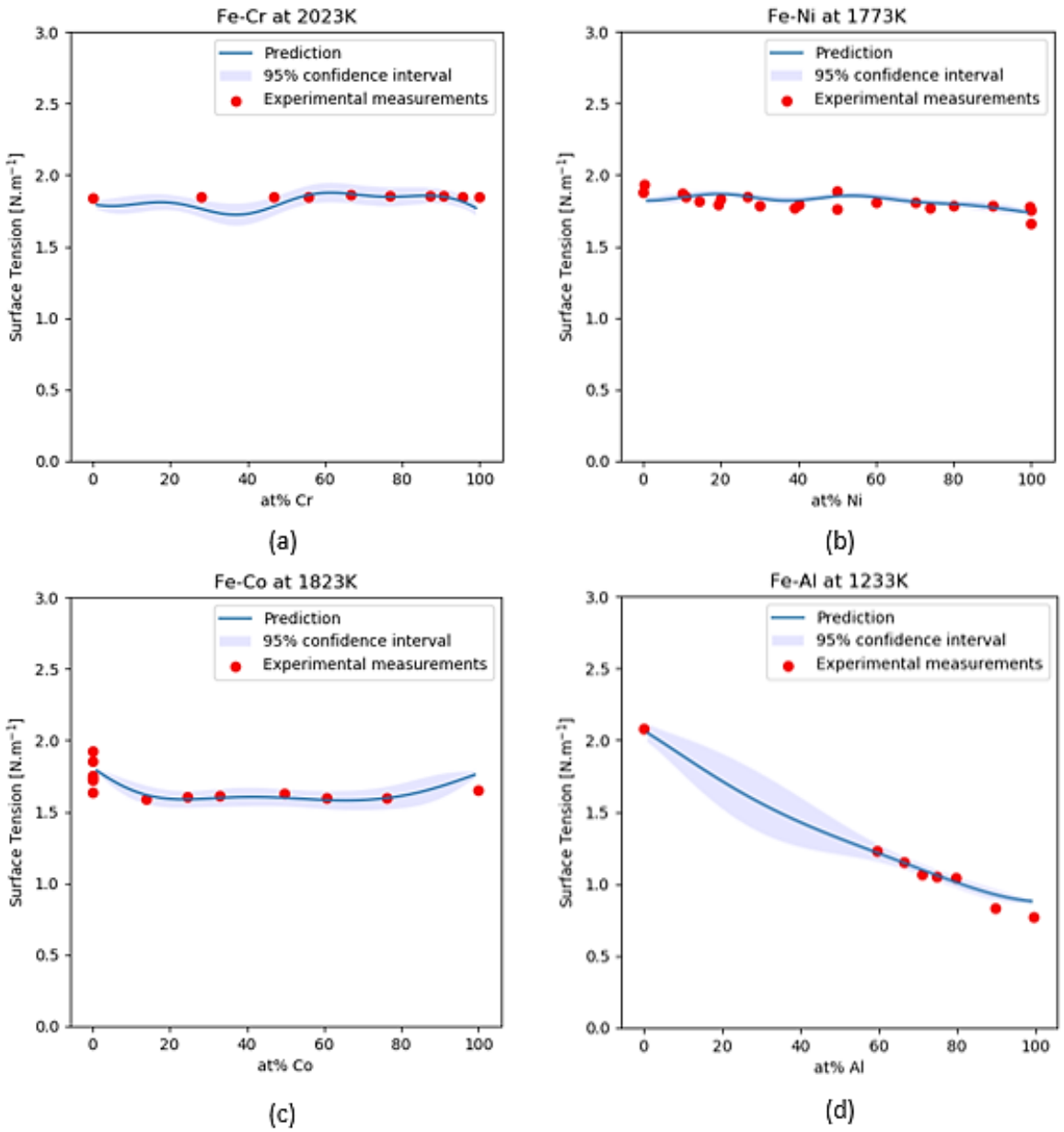

Figure 3 Surface tension prediction for a) Fe-Cr at 2023 K, b) Fe-Ni at 1873 K c) Fe-Co at 1823 K and d) Fe-Al at 1233 K

Several singular points need to be stressed on. Fig. 3 b and Fig. 4 a (Fe-Ni, Al-Cu, respectively) show the cases of well-documented alloys, with a wide experimental data set, coming from several research groups and sometimes, obtained by different experimental methods, and leading naturally to some differences in measured values. Obviously, the model prediction in such a situation should choose an "average" value, best optimized in the sense of existing trend, as observed in the figures. Another case is shown in Fig. 3 c (Fe-Co): for the studied temperature (1823 K), different ST values for pure Fe have been measured, with differences as large as 0.35 $N.m^{-1}$. It is reassuring to note that the model prediction of ST follows the data coming from the same bibliographic reference as the major part of data describing the whole Fe-Co binary system. Finally, the "bad" prediction of ST in Al-Ni system (Fig. 4 b) for almost equimolar alloys may be surprising. In fact, an almost constant ST value was measured for alloys containing between 45 and 75 at. % Ni [59] while the model indicates a continuous increase of ST with increasing Ni content. It may be hypothesized that the congruent solidification of NiAl B2-ordered phase and the associated liquid demixing in the vicinity of the equimolar composition [60] can change the liquid behavior; a phenomenon that would be at the origin of modified ST behavior, but not detected by the model, trained on homogeneous liquid behavior. Finally, we can see that the ST trends are successfully represented in the cases of Al-Cr at 2073 K and Al-Co at 1873 K (Fig. 4 c and d).

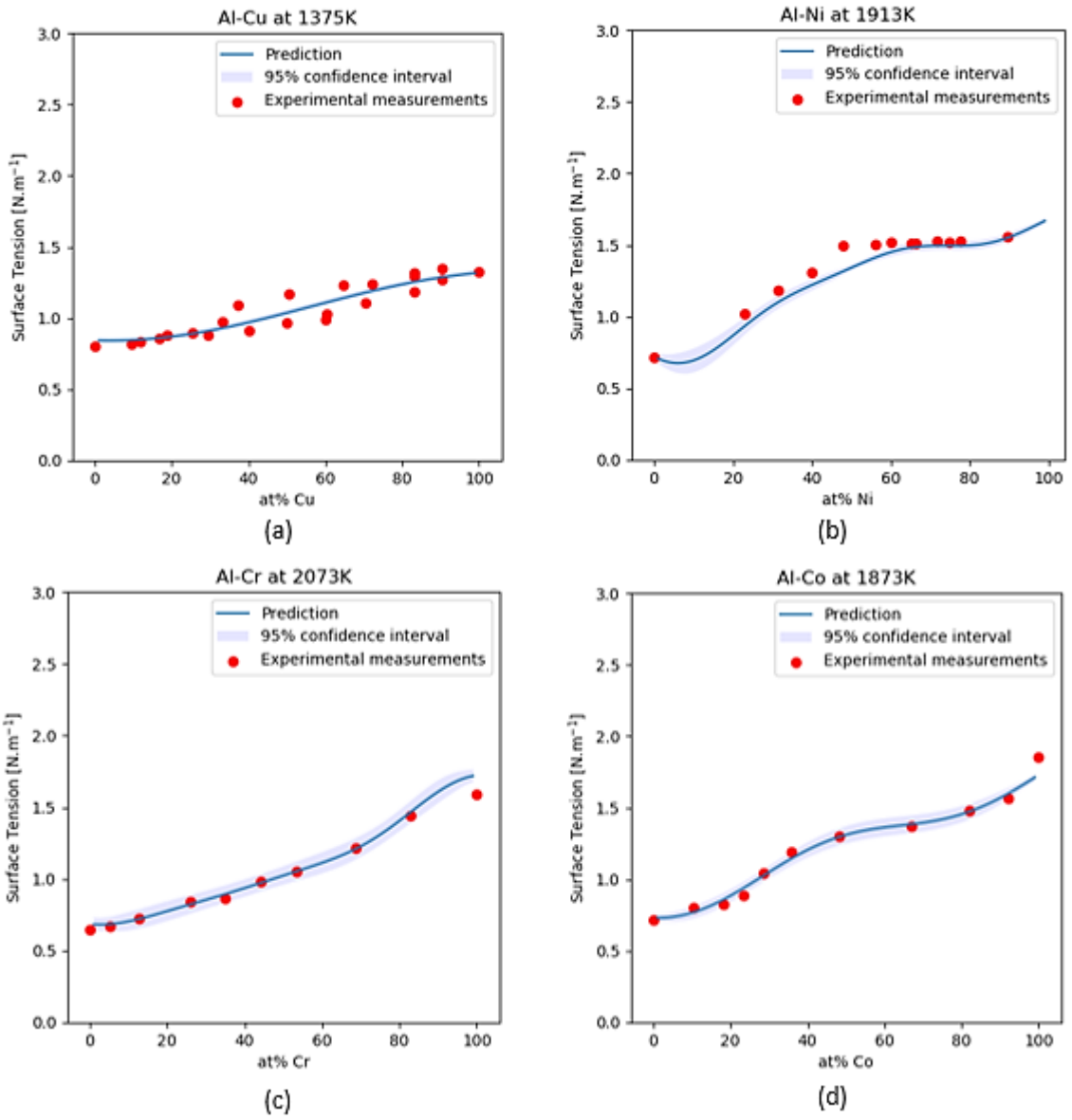

Figure 4 Surface tension prediction for a) Al-Cu at 1375 K b) Al-Ni at 1913 K c) Al-Cr at 2073 K and d) Al-Co at 1873 K

It is not surprising to find that the quality of predictions (measured by the standard deviation of predicted ST value) decreases in binary alloys if – for a large range of chemical compositions – experimental data is missing. Several cases are observed. In the Fe-Al binary system (Fig. 3d), experimental data are missing for alloys containing more than 40 at. % of Fe. The model

satisfactorily describes the Al-rich alloys; for the alloys containing more iron, the prediction follows an almost linear increase of ST, with an increase of standard deviation when compositions far from known experimental points are of concern. Yet, in all cases, the standard deviation is below 0.25 $N.m^{-1}$ and so, remains satisfactory. The same rule of increase of standard deviation far from experimental points may be clearly observed in the Fe-Mo system, Fig. 5a, with similar values of maximal standard deviation and so, a prediction that remains sufficient for applicative purposes. However, a more complicated situation has to be described in the Fe-Ti system (Fig. 5b). Only scarce experimental data, limited to Ti content as low as 3 at. %, (already discussed in §3.1), are available. Lack of reference points leads to a peculiar behavior of the ML-GPR model: a deep minimum of ST for about 20 % of Ti and standard deviations higher than 0.5 $N.m^{-1}$.

This is one of the rare cases in which the proposed model seems to extrapolate with a very low level of confidence, towards areas not sufficiently covered by the database, although the description of actual data appears correct in the corresponding range. Somewhat similar although less dramatic situations have been also seen in Fe-Mo. In doubt of the validity of the model in the Fe-Ti system beyond ~3% Ti, it would be preferable not to use the model in Fe-based alloys containing more than a few percent titanium. Fortunately, very high concentrations of such elements are almost never used for alloys of this class of engineering materials.

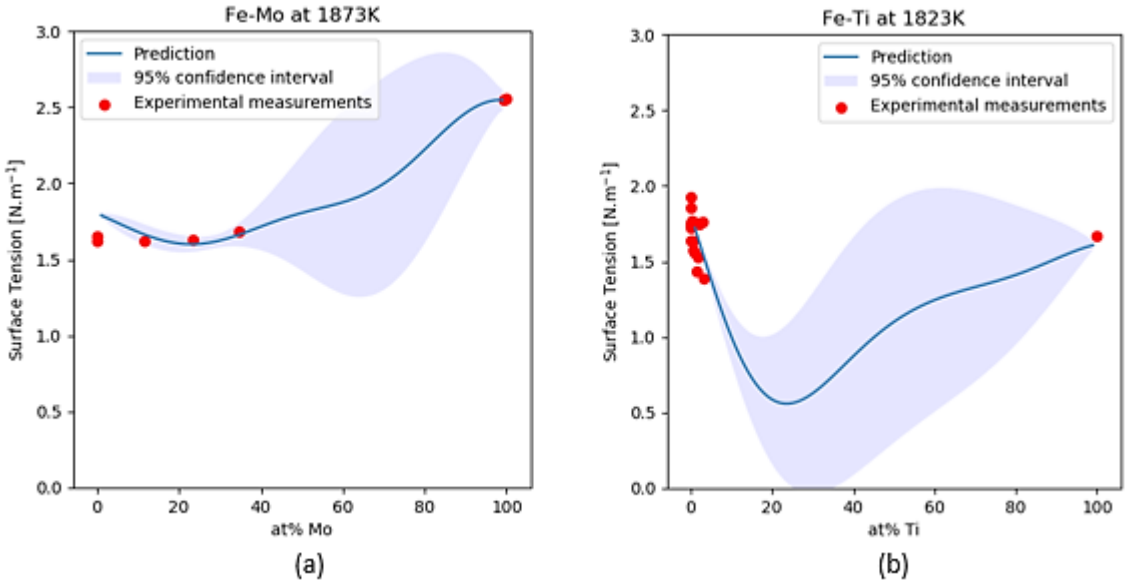

Figure 5 Surface tension prediction for a) Fe-Mo at 1873K and b) Fe-Ti at 1823K

3.3 Model evaluation: surface tension in ternary systems; comparison between experimental values and ML-GPR model prediction.

The ML-GPR model allows to evaluate the ST value for complete ternary maps in isothermal conditions. This permits a clear visualization of trends and the effect of different elements on ST values. In Fig. 6 ternary maps to describe the ST in several ternary systems are shown. The color code is used to identify the contours of ST value ($N.m^{-1}$). Unfortunately, the limited availability of data for ternary systems makes it difficult to evaluate the performance of the ML-GPR model globally. Although this is the case with binary systems as well, the evaluation of ternaries remains harder simply due to the fact that a higher number of points is needed to describe the space. Nevertheless, there has been some proposed thermodynamical models in the literature which predicted the ST for certain ternary systems. For example, Costa et al. [61] analyzed the energies of mixing in liquid Co–Cr, Cr–Ni and Co–Ni systems and extended the results to predict the

surface tension properties of the Co-Cr-Ni system. Compared to experimental data found in literature for the systems Cr-Ni and Co-Ni, their model predicts overestimated values of surface tension. Usually, this is explained by the high reactivity of alloy components and adsorption of oxygen on the liquid surface, which leads to a decrease in the surface tension and therefore a lower measured value compared to the theoretical prediction. Fig. 6 a. shows the surface tension prediction of the ML-GPR model for the Co-Cr-Ni system at 1873 K. Compared to the abovementioned thermodynamic model, the prediction of the ML-GPR model shows a slightly larger range of variation but similar trends. The difference in the exact values is explained by the fact that the model is trained on a set of experimental data; data that already include a certain range of error coming from material contamination, or experimental setup, etc. Similarly, Mehta et al. [62] studied the surface properties of the Fe-Cu-Si ternary system. They compared the results of four different models: Chou et al [63], Toop [64], Kohler [65] and Butler [33], which seem to be in agreement. Among the three components, pure silicon has the lowest surface tension value, and iron the highest. The surface tension of the ternary alloy changes non-linearly when viewed from the corners. The ML-GPR model's prediction for the Fe-Cu-Si system at 1773 K is shown in Fig. 6 b. The predictions are in excellent agreement with the results of [62], starting with a value around 1.7 $N.m^{-1}$ for the composition of $Si_5Cu_5Fe_{90}$, and decreasing as the content of Si and Cu increases, to reach a value around 0.9 $N.m^{-1}$ for the composition of $Si_{45}Cu_{45}Fe_{10}$, indicating the ability of the GPR model to interpolate/extrapolate surface tension values for ternary systems.

The main advantage of the machine learning model lies in its ability to generalize, without the need to study the exact systems involved and analyze the components that might be formed by the involved elements.

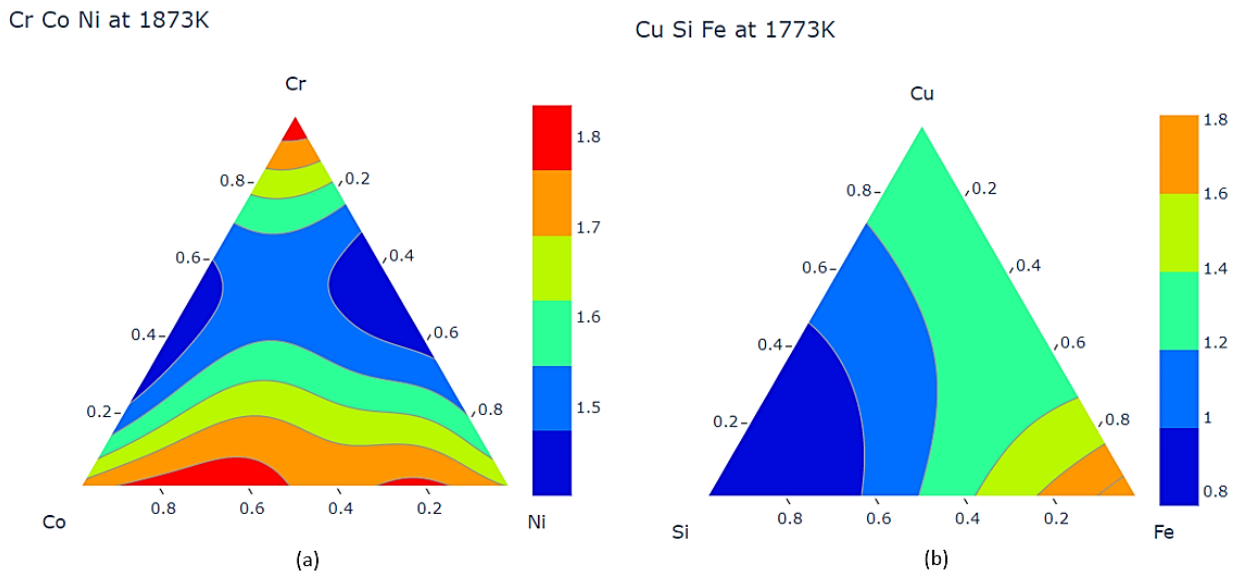

Figure 6 ML-GPR Prediction of Surface Tension [N.m^{-1}] for a) Cr-Co-Ni at 1873K and b) Cu-Si-Fe at 1773K

3.4. Efficiency of the ML-GPR model to describe multicomponent systems: comparison with existing data.

The next part of the work consisted in testing the ML-GPR model's ability to extrapolate towards multi-component (containing at least three elements) systems behavior, on the basis of data coming from simpler ones, since it has been built mainly from pure elements or binary systems, and to a minor extent from higher-order systems. To this purpose, training the ML-GPR model again on solely pure materials and binary alloys was done (~1770 data points). Then, the available experimental ST values of several ternaries and higher-order systems were used as test points. The results of model prediction in comparison with the experimental data from literature are shown in Fig. 7. To simplify, alloys from the same family; e.g., Al-Cu-Ag alloys, or Sn-Cu-Ag materials, were grouped by the same color. Due to the importance of stainless steels, and the existence of data for different grades of this class of materials, associated data take a significant place among

available studies, and they are divided into several classes for a better graphical representation in Fig. 7b. The exact chemical compositions of several grades of stainless steels [37] are summarized in Table 2 and used to build the graph in Fig. 7b.

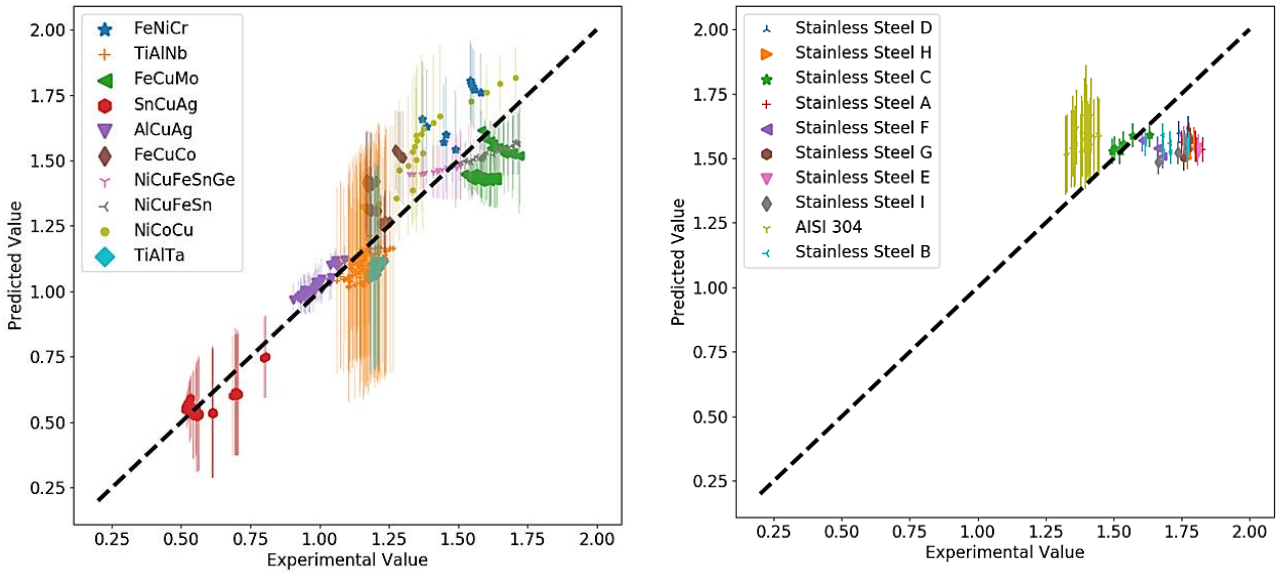

(a) (b)

Figure 7 ML-GPR model prediction vs experimental values of ST [N.m^{-1}] for several higher order system including several stainless steels grades (stainless steels A to I [40], AISI 304 [37]*), when the model is learnt solely from pure metals and binary alloys*

In general, it can be seen that the accuracy of prediction of ST by the ML-GPR model is satisfactory. For the ternary systems, like Al-Cu-Ag and Sn-Cu-Ag systems, the prediction accuracy is quite high. It is worth noting that the binaries of these systems are well represented in the database, compared to the other cases. Several datasets from literature describe both the effect of chemical composition and temperature for the Ag-Cu, Sn-Cu and Ag-Sn systems. As for the prediction of the quaternary $CuFeNi_{85}Sn$ (purple) and quinary $CuFeGeNi_{80}Sn$ (red), although the ML-GPR model correctly predicts the ST value, the predicted variation of temperature effects on ST seems unsatisfactory. By looking at the ST values of different binary systems containing

germanium, one can see that this element usually strongly decreases the ST value as it has low ST value itself, around 0.6 $N.m^{-1}$ at melting temperature. For example, a Ni-Ge alloy with 5% of Ge at 1873 K has an ST of 1.6 $N.m^{-1}$, compared to 1.75 $N.m^{-1}$ for pure Ni. Similarly, for Fe-Ge at 1823 K, an addition of 20% of Ge can decrease the ST value to 1.3 $N.m^{-1}$ compared to an average value of 1.8 $N.m^{-1}$ for pure Fe. This data allows the model to give a proper estimation of the ST but is not enough for a satisfactory estimation of the temperature effect. As for the Ni-Co-Cu system, an opposite behavior is observed. The predicted values slightly overestimate the measured ST value. In fact, for the Ni-Co binary system we saw that there is little to no effect of composition on ST. In the case of Ni-Cu and Co-Cu, the addition of Cu decreases the ST. The results are therefore somewhat surprising, as the model does not succeed to predict the effect of Cu, especially when it is present in low contents.

For different stainless steel compositions studied by Li et al. [37], Table 2, and the Fe-Cu-Mo system studied in [66], the ML-GPR model slightly underestimates the ST value. The opposite is seen for some data concerning an AISI 304 steel measured by the maximum bubble method. Let us note that for the same alloy measured with sessile drop method, we do not observe a high error for the model predictions. This part of the study intended to assess whether a model built only from low order systems (unaries and binaries) would be able to give fair values and/or trends for higher order systems, i.e. ternaries or even more complex alloys. Let us stress on the fact that, even if the trends are slightly degraded for commercial alloys (eg.: stainless steels), good value ranges are obtained for all alloys.

Steel	C	Si	Mn	Al	Cr	Ti
A	0.0435	0.287	0.189	0.1288	16.198	0.0044
B	0.0847	0.298	0.596	0.089	15.995	0.0056
C	0.0689	0.316	0.572	0.0042	16.232	0.0028
D	0.0084	0.464	0.35	0.0562	10.858	0.2211

E	0.0056	0.126	0.141	0.0504	16.199	0.293
F	0.0053	0.092	0.112	0.0806	17.346	0.2741
G	0.0059	0.145	0.131	0.052	18.67	0.1541
H	0.0153	0.555	0.149	0.0216	19.105	0.0082
I	0.0076	0.467	0.124	0.0293	21.511	0.0042

Table 2 Composition of different grades of stainless steel in weight % [37]

Therefore, it may be reasonably expected that no further significant degradation of prediction would come for the complete model and it seems possible to extend the model to higher-order systems, as long as the compositional space of the lower order systems involved is sufficiently well described. The range to which it can be extrapolated could be individually discussed based on the statistical representation of the system on topic, but also with the help of the error bars provided by the algorithm. Consequently, the model learnt using all available data should be able to provide fair predictions of the ST in the case of multicomponent alloys, which is attempted in the next section.

3.5 Use of the ML-GPR model to predict ST in complex alloys: application to austenitic HEA alloys

Alloy	**$T_{liquidus}$ in K**	**Surface Tension [$N.m^{-1}$]**
CuCrFeMoNi	1816	1.39
Al0.5CrCuFeNi2	1561	1.47
Al0.5CrCuFeNi	1657	1.34
CoCrFeMnNi	1596	1.2
CoCrFeNi	1713	1.4
CrFeMnNi	1574	1.0
CoCuFeMnNi	1555	1.12
CoCrCuFeNi	1648	1.23
CrCuFeMoNi	1817	1.39

Al0.5CoCrCu0.5FeNi	1607	1.3
Al0.3CoCrCuFeNi	1620	1.28
Al0.5CoCrCuFeNi	1599	1.27
Al0.5CoCrCu0.5Fe2Ni	1644	1.22
Al0.5CoCrCu0.5Fe3Ni	1670	1.21
Al0.5CoCrCu0.5Fe3.5Ni	1680	1.22
CoCrFeMo0.3Ni	1674	1.4
Al0.3CoCrFeMo0.1Ni	1654	1.37
Al0.2CrCuFeNi2	1589	1.48
Al0.6CrCuFeNi2	1552	1.46
Al0.25CoCrFeNi	1674	1.37
Al0.3CoCrFeNi	1666	1.36
Al0.375CoCrFeNi	1652	1.35

Table 3 Predicted surface tension values for some HEA alloys at their melting point

In the next part of the study, the ML-GPR model, learnt from all available data (retrained on the whole database), was used to predict the surface tension of several alloys for which experimental data are still missing. Such an approach, even if it would come along with a high level of uncertainty on the predicted values, is valuable in the framework of alloy design. Indeed, decreasing the ST value may be of interest in some specific processes such as welding or additive manufacturing, to help the stabilization of the meltpool. However little knowledge of the trend of ST variations with composition is known in the case of highly alloyed systems. This section provides a quick glance of possible variations to foresee some possible research directions where ST at the liquidus could be possibly minimized. This investigation will give further insight into the effect of several elements on the value of the ST, as well as the behavior of the material at different temperatures. In Table 3 the surface tension for several face-centered cubic (FCC) high entropy alloys (HEA) [67] is given at their liquidus temperatures estimated using ThermoCalc software (TCHEA4 database). It is clear that the range of variation seems to be limited. It has been mentioned that certain elements can have a similar effect on the trend of the ST value in a specific

system, such as the behavior of transition metal elements in a binary system with iron [27]. Nevertheless, the results show that by varying the content of one element or the other, it is possible to optimize the value of ST depending on the desired outcome. For example, changing the composition of the CoCuFeNi equimolar alloy by decreasing the amount of either nickel or cobalt, could help achieve a minimum in the ST value. Similarly, for the CoCrFeNi equimolar alloy, introducing a small amount of aluminum could also decrease slightly the value of ST.

An example of ML-GPR model predictions is given in Fig. 8 for the CoCrFeMnNi equimolar alloy (also known as Cantor alloy). The effect of the different elements on the ST value of the alloy is presented by considering that the element is added to an equimolar quaternary alloy. The square points represent the surface tension values for the quaternary alloys CoCrFeNi (in red), CrFeMnNi (in blue), CoFeMnNi (in green), CoCrFeMn (in pink) and CoCrMnNi (in orange). The predicted ST value for the Cantor alloy is in fact surprisingly low, not far from the minimum value obtained for a major part of studied compositions. One explanation could be come from a high amount of manganese in Cantor alloy: as presented in Fig. 8, this element has a strong effect on ST values in the studied system. More generally, Mn is the first predominant factor driving the global ST variations. When Mn content increases, the ST value decreases progressively. For the other elements, the trend is opposed, because it results in a lower Mn fraction. However, a second predominant factor is the liquidus temperature, which is also affected by composition. For instance, the addition of Fe results in an increase of liquidus temperature from 1277°C for CoCrMnNi to 1538°C for pure Fe. For these elements, the temperature results in a decrease of ST value according to the ST database. Therefore, the variation from Cantor to a pure element should result in a higher liquidus temperature, and a lower ST. The competition between these two opposite effects may eventually result in a sag point, as it is the case for Fe curve. On the other

hand, in the case of Ni content (denominated "x" in the following), the CoCrFeMn alloy has a liquidus at 1373°C, and the variation of liquidus is only of 82°C when x changes from 0 to 100. Therefore, liquidus has a limited impact on ST in this case, and ST is mostly driven by Mn content, with a continuous decrease when x tends toward 0. This explains the peculiar behavior of Ni curve at low x values.

These preliminary results are based on the information acquired from the existing database. The extrapolation of the model to multicomponent alloys induces a relatively large variance interval of more than 0.3 $N.m^{-1}$, as the predicted systems are farther from trained input samples in the composition space. Of course, the more data is added to the training database, the better the model performs on the different aspects discussed. Nevertheless, this model represents a simple method to estimate a range for the ST value and trend without the complication of manually calculating physical parameters for the elements and their interactions. This is especially useful in cases where the aim is to optimize the property rather than achieve a specific value.

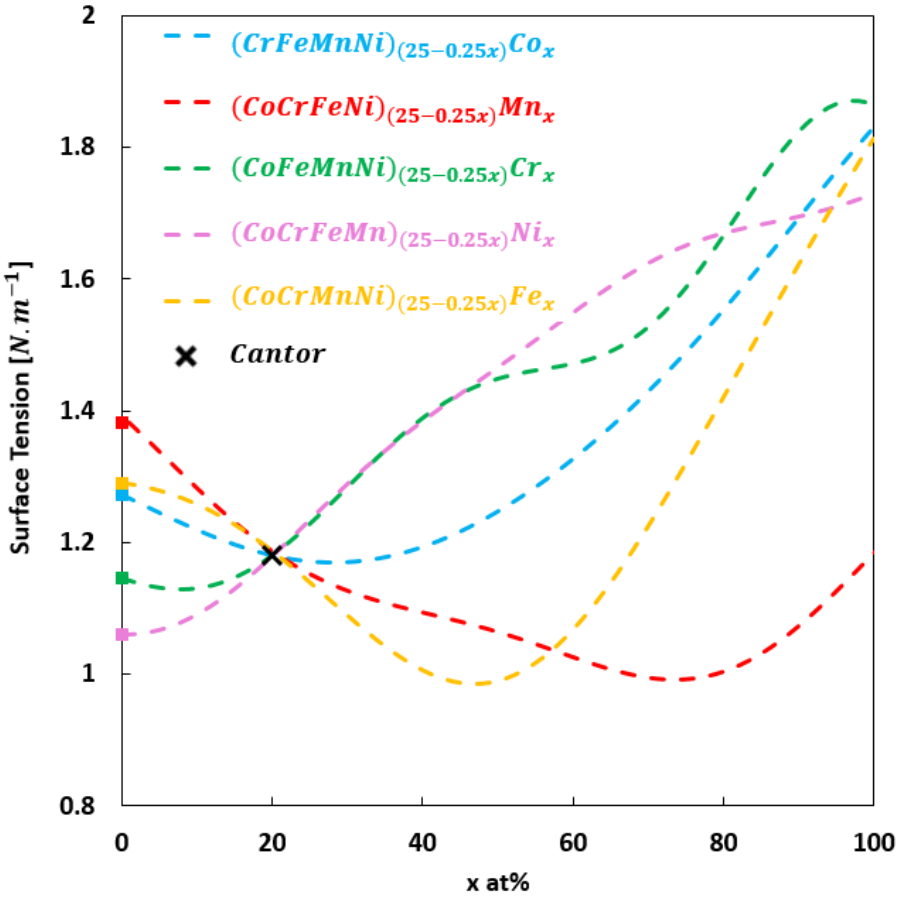

Figure 8 ML-GPR model prediction of surface tension values, showing the independent effects of elements on the equimolar alloy CoCrFeMnNi (Cantor alloy) behavior. Calculations performed at melting temperature of each alloy, estimated from ThermoCalc data.

4. Conclusion

1. With a long-term purpose of improvement of criteria of alloy design for innovating processes like additive manufacturing, a Machine-Learning model based on Gaussian Process Regression (ML-GPR) was developed for predicting the surface tension values in metallic alloys. The model is built on the basis of the data coming from experimental measurements found. Analysis of more than 70 papers and textbooks allowed the creation of a database containing more than 2200

experimental points. An interesting perspective would be to incorporate data obtained by atomistic simulation.

2. The model's database comes mainly from pure elements and simple alloys, mostly binary and, less commonly, containing three or more chemical elements. A good agreement between prediction and experiments was generally observed in binary and ternary alloys when enough experimental data exist. The confidence range of prediction is generally lower than 0.2 $N.m^{-1}$. There are rare cases in which the model seems to extrapolate with a very low level of confidence, towards areas not sufficiently covered by the database, such as in Fe-Ti or Fe-Mo systems.

3. On the basis of results for simple alloys, the possibilities of extension of predictions by ML-GPR model to multi-element alloys have been assessed.

4. The tentative of using the ML-GPR model to predict the surface tension in novel concentrated alloys, namely austenitic HEAs from the CoCrFeMnNi family, remains a challenging task. Yet, significant variations in ST could be identified when changing the contents in certain elements. Especially, a strong effect of Mn, decreasing the ST values, was shown.

References

[1] N. T. Aboulkhair, M. Simonelli, L. Parry, I. Ashcroft, C. Tuck, and R. Hague, "3D printing of Aluminium alloys: Additive Manufacturing of Aluminium alloys using selective laser melting," *Prog. Mater. Sci.*, vol. 106, no. July, p. 100578, 2019, doi: 10.1016/j.pmatsci.2019.100578.

[2] E. O. Olakanmi, R. F. Cochrane, and K. W. Dalgarno, "A review on selective laser sintering/melting (SLS/SLM) of aluminium alloy powders: Processing, microstructure, and properties," *Prog. Mater. Sci.*, vol. 74, pp. 401–477, 2015, doi: 10.1016/j.pmatsci.2015.03.002.

[3] T. DebRoy *et al.*, "Additive manufacturing of metallic components – Process, structure and properties," *Prog. Mater. Sci.*, vol. 92, pp. 112–224, 2018, doi: 10.1016/j.pmatsci.2017.10.001.

[4] C. Y. Yap *et al.*, "Review of selective laser melting: Materials and applications," *Appl. Phys. Rev.*, vol. 2, no. 4, 2015, doi: 10.1063/1.4935926.

[5] D. Herzog, V. Seyda, E. Wycisk, and C. Emmelmann, "Additive manufacturing of metals," *Acta Mater.*, vol. 117, pp. 371–392, 2016, doi: 10.1016/j.actamat.2016.07.019.

[6] W. J. Sames, F. A. List, S. Pannala, R. R. Dehoff, and S. S. Babu, "The metallurgy and processing science of metal additive manufacturing," *Int. Mater. Rev.*, vol. 61, no. 5, pp. 315–360, 2016, doi: 10.1080/09506608.2015.1116649.

[7] T. Fuhrich, P. Berger, and H. Hügel, "Marangoni effect in laser deep penetration welding of steel," *J. Laser Appl.*, vol. 13, no. 5, pp. 178–186, 2001, doi: 10.2351/1.1404412.

[8] M. D. L. Christian Wohlfarth, B. Wohlfarth, *Surface Tension of Pure Liquids and Binary Liquid Mixtures*. Springer, 1997.

[9] C. J. Smithells, "Metals reference book," *J. Less Common Met.*, vol. 51, no. 2, pp. 354–355, 1977, doi: 10.1016/0022-5088(77)90096-0.

[10] K. C. Mills and Y. C. Su, "Review of surface tension data for metallic elements and alloys: Part 1 - Pure metals," *Int. Mater. Rev.*, vol. 51, no. 6, pp. 329–351, 2006, doi: 10.1179/174328006X102510.

[11] B. J. Keene, "Review of data for the surface tension of pure metals," *Int. Mater. Rev.*, vol. 38, no. 4, pp. 157–192, 1993, doi: 10.1179/imr.1993.38.4.157.

[12] A. Kasama, A. McLean, W. A. Miller, Z. Morita, and M. J. Ward, "Surface tension of liquid iron and iron-oxygen alloys," *Can. Metall. Q.*, vol. 22, no. 1, pp. 9–17, 1983, doi: 10.1179/cmq.1983.22.1.9.

[13] H. M. Lu and Q. Jiang, "Surface tension and its temperature coefficient for liquid metals," *J. Phys. Chem. B*, vol. 109, no. 32, pp. 15463–15468, 2005, doi: 10.1021/jp0516341.

[14] P. Sahoo, T. Debroy, and M. J. McNallan, "Surface tension of binary metal-surface active solute systems under conditions relevant to welding metallurgy," *Metall. Trans. B*, vol. 19, no. 2, pp. 483–491, 1988, doi: 10.1007/BF02657748.

[15] B. J. Keene, K. C. Mills, J. W. Bryant, and E. D. Hondros, "Effects of interaction between surface active elements on the surface tension of iron," *Can. Metall. Q.*, vol. 21, no. 4, pp. 393–403, 1982, doi: 10.1179/cmq.1982.21.4.393.

[16] F. A. Halden and W. D. Kingery, "Surface tension at elevated temperatures. II. Effect of

C, N, O and S on liquid iron surface tension and interfacial energy with Al2O3," *J. Phys. Chem.*, vol. 59, no. 6, pp. 557–559, 1955, doi: 10.1021/j150528a018.

[17] H. G. Kim, J. Choe, T. Inoue, S. Ozawa, and J. Lee, "Surface Tension of Super-Cooled Fe-O Liquid Alloys," *Metall. Mater. Trans. B Process Metall. Mater. Process. Sci.*, vol. 47, no. 4, pp. 2079–2081, 2016, doi: 10.1007/s11663-016-0712-z.

[18] J. Zhu and K. Mukai, "The surface tension of liquid iron containing nitrogen and oxygen," *ISIJ Int.*, vol. 38, no. 10, pp. 1039–1044, 1998, doi: 10.2355/isijinternational.38.1039.

[19] I. Takamichi and I. L. G. Roderick, *The Thermophysical Properties of Metallic Liquids Volume 2: Predictive Models*. Oxford University Press, 2015.

[20] A. J. B. Milne, B. Defez, M. Cabrerizo-Vílchez, and A. Amirfazli, "Understanding (sessile/constrained) bubble and drop oscillations," *Adv. Colloid Interface Sci.*, vol. 203, pp. 22–36, 2014, doi: 10.1016/j.cis.2013.11.006.

[21] V. B. Fainerman and R. Miller, "The maximum bubble pressure tensiometry," in *Drops and bubbles in interfacial research*, D. MÖbius and R. Miller, Eds. Elsevier, 1998, pp. 279–326.

[22] V. B. Fainerman and R. Miller, "Maximum bubble pressure tensiometry—an analysis of experimental constraints," *Adv. Colloid Interface Sci.*, vol. 108–109, pp. 287–301, May 2004, doi: 10.1016/j.cis.2003.10.010.

[23] J. W. Gibbs, "The collected works of J. Williard Gibbs," vol. 1, pp. 219–331, 1928.

[24] E. A. Guggenheim, "Statistical thermodynamics of the surface of a regular solution," *Trans. Faraday Soc.*, vol. 41, p. 150, 1945, doi: 10.1039/tf9454100150.

[25] E. A. Guggenheim and N. K. Adam, “The Thermodynamics of Adsorption at the Surface of Solutions,” vol. 1, 1932.

[26] J. A. V Butler, “The thermodynamics of the surfaces of solutions,” *Proc. R. Soc. London. Ser. A, Contain. Pap. a Math. Phys. Character*, vol. 135, no. 827, pp. 348–375, Mar. 1932, doi: 10.1098/rspa.1932.0040.

[27] M. Vermot des Roches, A. E. Gheribi, and P. Chartrand, “A versatile multicomponent database for the surface tension of liquid metals,” *Calphad Comput. Coupling Phase Diagrams Thermochem.*, vol. 65, no. April, pp. 326–339, Jun. 2019, doi: 10.1016/j.calphad.2019.04.002.

[28] P. Wynblatt, A. Saúl, and D. Chatain, “The effects of prewetting and wetting transitions on the surface energy of liquid binary alloys,” *Acta Mater.*, vol. 46, no. 7, pp. 2337–2347, Apr. 1998, doi: 10.1016/S1359-6454(98)80015-3.

[29] I. Egry, “The surface tension of binary alloys: Simple models for complex phenomena,” *Int. J. Thermophys.*, vol. 26, no. 4, pp. 931–939, 2005, doi: 10.1007/s10765-005-6675-y.

[30] I. Egry, E. Ricci, R. Novakovic, and S. Ozawa, “Surface tension of liquid metals and alloys — Recent developments,” *Adv. Colloid Interface Sci.*, vol. 159, no. 2, pp. 198–212, Sep. 2010, doi: 10.1016/j.cis.2010.06.009.

[31] A. E. Gheribi, M. Vermot des Roches, and P. Chartrand, “Modelling the surface tension of liquid metals as a function of oxygen content,” *J. Non. Cryst. Solids*, vol. 505, no. July 2018, pp. 154–161, 2019, doi: 10.1016/j.jnoncrysol.2018.10.006.

[32] G. Kaptay, “Improved Derivation of the Butler Equations for Surface Tension of

Solutions," *Langmuir*, vol. 35, no. 33, pp. 10987–10992, 2019, doi: 10.1021/acs.langmuir.9b01892.

[33] J. A. V Butler and P. R. S. L. A, "The thermodynamics of the surfaces of solutions," *Proc. R. Soc. London. Ser. A, Contain. Pap. a Math. Phys. Character*, vol. 135, no. 827, pp. 348–375, 1932, doi: 10.1098/rspa.1932.0040.

[34] J. Chang, H. P. Wang, K. Zhou, and B. Wei, "Surface tension measurement of undercooled liquid Ni-based multicomponent alloys," *Philos. Mag. Lett.*, vol. 92, no. 9, pp. 428–435, 2012, doi: 10.1080/09500839.2012.685768.

[35] A. Dogan and H. Arslan, "Thermophysical properties of Cu–In–Sn liquid Pb-free alloys: viscosity and surface tension," *Philos. Mag.*, vol. 98, no. 1, pp. 37–53, 2018, doi: 10.1080/14786435.2017.1392053.

[36] Z. Guo, M. Hindler, W. Yuan, and A. Mikula, "The density and surface tension of In-Sn and Cu-In-Sn alloys," *Monatshefte fur Chemie*, vol. 142, no. 6, pp. 579–584, 2011, doi: 10.1007/s00706-011-0501-y.

[37] Z. Li, K. Mukai, M. Zeze, and K. C. Mills, "Determination of the surface tension of liquid stainless steel," *J. Mater. Sci.*, vol. 40, pp. 2191–2195, 2005.

[38] J. Choe *et al.*, "Surface tension measurements of 430 stainless steel," *ISIJ Int.*, vol. 54, no. 9, pp. 2104–2108, 2014, doi: 10.2355/isijinternational.54.2104.

[39] Y. Su, Z. Li, and K. C. Mills, "Equation to estimate the surface tensions of stainless steels," *J. Mater. Sci.*, vol. 40, no. 9–10, pp. 2201–2205, 2005, doi: 10.1007/s10853-005-1933-8.

[40] M. Hayashi, A. Jakobsson, T. Tanaka, and S. Seetharaman, “Surface tension of the nickel-based superalloy CMSX-4,” *High Temp. - High Press.*, vol. 35–36, no. 4, pp. 441–445, 2003, doi: 10.1068/htjr123.

[41] R. K. Wunderlich, H. J. Fecht, and G. Lohöfer, “Surface Tension and Viscosity of the Ni-Based Superalloys LEK94 and CMSX-10 Measured by the Oscillating Drop Method on Board a Parabolic Flight,” *Metall. Mater. Trans. B Process Metall. Mater. Process. Sci.*, vol. 48, no. 1, pp. 237–246, 2017, doi: 10.1007/s11663-016-0847-y.

[42] B. B. Alchagirov, R. K. Arkhestov, F. F. Dyshekova, and T. M. Taova, “Surface tension of alloys with additives of alkali metals,” *High Temp.*, vol. 51, no. 2, pp. 183–196, 2013, doi: 10.1134/S0018151X13020016.

[43] P. F. Paradis, T. Ishikawa, and S. Yoda, “Non-Contact Measurements of Surface Tension and Viscosity of Niobium, Zirconium, and Titanium Using an Electrostatic Levitation Furnace,” *Int. J. Thermophys.*, vol. 23, no. 3, pp. 825–842, 2002, doi: 10.1023/A:1015459222027.

[44] K. Monma and H. Suto, “Experimental Studies on the Surface Tension of Molten Metals and Alloys,” *Trans. JIM*, vol. 1, no. 2, pp. 69–76, 1960, doi: 10.2320/matertrans1960.1.69.

[45] J. Brillo and I. Egry, “Surface tension of nickel , copper , iron,” *Calphad Comput. Coupling Phase Diagrams Thermochem.*, vol. 0, pp. 2213–2216, 2005.

[46] F. Tancret, I. Toda-Caraballo, E. Menou, and P. E. J. Rivera Díaz-Del-Castillo, “Designing high entropy alloys employing thermodynamics and Gaussian process statistical analysis,” *Mater. Des.*, vol. 115, pp. 486–497, 2017, doi: 10.1016/j.matdes.2016.11.049.

[47] S. Chibani and F. X. Coudert, “Machine learning approaches for the prediction of materials properties,” *APL Mater.*, vol. 8, no. 8, 2020, doi: 10.1063/5.0018384.

[48] K. Rajan, “Materials informatics,” *Mater. Today*, vol. 8, no. 10, pp. 38–45, 2005, doi: 10.1016/S1369-7021(05)71123-8.

[49] Y. Liu, T. Zhao, W. Ju, S. Shi, S. Shi, and S. Shi, “Materials discovery and design using machine learning,” *J. Mater.*, vol. 3, no. 3, pp. 159–177, 2017, doi: 10.1016/j.jmat.2017.08.002.

[50] H. Yamada *et al.*, “Predicting Materials Properties with Little Data Using Shotgun Transfer Learning,” *ACS Cent. Sci.*, vol. 5, no. 10, pp. 1717–1730, 2019, doi: 10.1021/acscentsci.9b00804.

[51] G. Pilania, C. Wang, X. Jiang, S. Rajasekaran, and R. Ramprasad, “Accelerating materials property predictions using machine learning,” *Sci. Rep.*, vol. 3, no. 1, p. 2810, Dec. 2013, doi: 10.1038/srep02810.

[52] L. Ward, A. Agrawal, A. Choudhary, and C. Wolverton, “A general-purpose machine learning framework for predicting properties of inorganic materials,” *npj Comput. Mater.*, vol. 2, no. 1, p. 16028, Nov. 2016, doi: 10.1038/npjcompumats.2016.28.

[53] Z.-L. Wang and Y. Adachi, “Property prediction and properties-to-microstructure inverse analysis of steels by a machine-learning approach,” *Mater. Sci. Eng. A*, vol. 744, pp. 661–670, Jan. 2019, doi: 10.1016/j.msea.2018.12.049.

[54] C. A. L. Bailer-Jones, H. K. D. H. Bhadeshia, and D. J. C. MacKay, “Gaussian process modelling of austenite formation in steel,” *Mater. Sci. Technol.*, vol. 15, no. 3, pp. 287–

294, Mar. 1999, doi: 10.1179/026708399101505851.

[55] S. Bishnoi, R. Ravinder, H. S. Grover, H. Kodamana, and N. M. A. Krishnan, "Scalable Gaussian processes for predicting the optical, physical, thermal, and mechanical properties of inorganic glasses with large datasets," *Mater. Adv.*, vol. 2, no. 1, pp. 477–487, 2021, doi: 10.1039/D0MA00764A.

[56] H. Rappel, L. A. A. Beex, L. Noels, and S. P. A. Bordas, "Identifying elastoplastic parameters with Bayes' theorem considering output error, input error and model uncertainty," *Probabilistic Eng. Mech.*, vol. 55, pp. 28–41, Jan. 2019, doi: 10.1016/j.probengmech.2018.08.004.

[57] C. E. Rasmussen and C. K. I. Williams, *Gaussian Processes for Machine Learning*. 2006.

[58] F. Pedregosa *et al.*, "Scikit-learn: Machine Learning in Python," *J. Mach. Learn. Res.*, vol. 12, pp. 2825–2830, 2011.

[59] V. Eremenko, Y. N. Ivashchenko, and P. Marsenyuk, "Free surface energy and density of liquid vanadium, niobium, and tantalum at the melting point," *High Temp.*, vol. 22, no. 4, pp. 705–708, 1984.

[60] F. Baras and O. Politano, "Molecular dynamics simulations of nanometric metallic multilayers: Reactivity of the Ni-Al system," *Phys. Rev. B*, vol. 84, no. 2, p. 024113, Jul. 2011, doi: 10.1103/PhysRevB.84.024113.

[61] C. Costa, S. Delsante, G. Borzone, D. Zivkovic, and R. Novakovic, "Thermodynamic and surface properties of liquid Co-Cr-Ni alloys," *J. Chem. Thermodyn.*, vol. 69, pp. 73–84, 2014, doi: 10.1016/j.jct.2013.09.034.

[62] U. Mehta, S. K. Yadav, I. Koirala, R. P. Koirala, G. K. Shrestha, and D. Adhikari, "Study of surface tension and viscosity of Cu–Fe–Si ternary alloy using a thermodynamic approach," *Heliyon*, vol. 6, no. 8, p. e04674, Aug. 2020, doi: 10.1016/j.heliyon.2020.e04674.

[63] K. C. Chou, "A general solution model for predicting ternary thermodynamic properties," *Calphad*, vol. 19, no. 3, pp. 315–325, 1995, doi: 10.1016/0364-5916(95)00029-E.

[64] G. W. Toop, "Predicting ternary activities using binary data," *Trans Met. Soc AIME*, vol. 233, no. 5, pp. 850–855, 1965.

[65] F. Kohler, "Daten eines ternären Systems aus den zugehörigen binären Systemen," *Monatshefte für Chemie*, vol. 91, no. 4, pp. 738–740, 1960, doi: 10.1007/BF00899814.

[66] H. P. Wang, B. C. Luo, T. Qin, J. Chang, and B. Wei, "Surface tension of liquid ternary Fe-Cu-Mo alloys measured by electromagnetic levitation oscillating drop method," *J. Chem. Phys.*, vol. 129, no. 12, 2008, doi: 10.1063/1.2981833.

[67] Y. F. Ye, Q. Wang, J. Lu, C. T. Liu, and Y. Yang, "High-entropy alloy: challenges and prospects," *Mater. Today*, vol. 19, no. 6, pp. 349–362, 2016, doi: 10.1016/j.mattod.2015.11.026.

[68] K. Nogi, "Surface Tension of Liquid Fe-(Cu, Sn, Cr) and Ni-(Cu, Sn) Binary alloys," *Mater. Transcations*, vol. 32, pp. 164–168, 1991.

[69] K. Mori, M. Kishimoto, T. Shimose, and Y. Kawai, "Surface Tension of Liquid Iron-Nickel-Chromium Alloy System," *J. Japan Inst. Met.*, vol. 39, no. 12, pp. 1301–1307, 1975, doi: 10.2320/jinstmet1952.39.12_1301.

[70] I. I. Egry and J. J. Brillo, “Surface Tension and Density of Liquid Metallic Alloys Measured by Electromagnetic Levitation,” *J. Chem. Eng. Data*, vol. 54, no. 9, pp. 2347–2352, Sep. 2009, doi: 10.1021/je900119n.

[71] D. Giuranno, A. Tuissi, R. Novakovic, and E. Ricci, “Surface tension and density of Al-Ni alloys,” *J. Chem. Eng. Data*, vol. 55, no. 9, pp. 3024–3028, 2010, doi: 10.1021/je901055j.

[72] I. Egry, J. Brillo, D. Holland-Moritz, and Y. Plevachuk, “The surface tension of liquid aluminium-based alloys,” *Mater. Sci. Eng. A*, vol. 495, no. 1–2, pp. 14–18, Nov. 2008, doi: 10.1016/j.msea.2007.07.104.

[73] F. Xiao, L. xiao Liu, R. hui Yang, H. kai Zhao, L. Fang, and C. Zhang, “Surface tension of molten Ni-(Cr, Co, W) alloys and segregation of elements,” *Trans. Nonferrous Met. Soc. China (English Ed.*, vol. 18, no. 5, pp. 1184–1188, 2008, doi: 10.1016/S1003-6326(08)60202-2.

[74] J. J. Wessing and J. Brillo, “Density, Molar Volume, and Surface Tension of Liquid Al-Ti,” *Metall. Mater. Trans. A Phys. Metall. Mater. Sci.*, vol. 48, no. 2, pp. 868–882, Feb. 2017, doi: 10.1007/s11661-016-3886-8.

[75] J. Schmitz, J. Brillo, I. Egry, and R. Schmid-Fetzer, “Surface tension of liquid Al–Cu binary alloys,” vol. 100, no. 11, pp. 1529–1535, doi: 10.3139/146.110221.

[76] P. Laty, J. C. Joud, P. Desré, and G. Lang, “Tension superficielle d’alliages liquides aluminium-cuivre,” *Surf. Sci.*, vol. 69, no. 2, pp. 508–520, 1977, doi: 10.1016/0039-6028(77)90130-3.

[77] H. Kobatake, J. Brillo, J. Schmitz, and P. Y. Pichon, “Surface tension of binary Al–Si

liquid alloys," *J. Mater. Sci.*, vol. 50, no. 9, pp. 3351–3360, 2015, doi: 10.1007/s10853-015-8883-6.

[78] I. F. Bainbridge and J. A. Taylor, "The surface tension of pure aluminum and aluminum alloys," *Metall. Mater. Trans. A Phys. Metall. Mater. Sci.*, vol. 44, no. 8, pp. 3901–3909, 2013, doi: 10.1007/s11661-013-1696-9.

[79] J. . Taylor, "The surface tensions of liquid-metal solutions," *Acta Metall.*, vol. 4, no. 5, pp. 460–468, 1956, doi: 10.1016/0001-6160(56)90042-6.

[80] A. Schneider and E. K. Stoll, "Zeitschrift für Elektrochemie und angewandte physikalische Chemie," 1941, doi: https://doi.org/10.1002/bbpc.19410470709.

[81] Y. V. Naidich, V. M. Perevertailo, and L. P. Obushchak, "Density and surface tension of alloys of the systems Au-Si and Au-Ge," *Sov. Powder Metall. Met. Ceram.*, vol. 14, no. 5, pp. 403–404, 1975, doi: 10.1007/BF00807814.

[82] J. Brillo and G. Kolland, "Surface tension of liquid Al–Au binary alloys," *J. Mater. Sci.*, vol. 51, no. 10, pp. 4888–4901, 2016, doi: 10.1007/s10853-016-9794-x.

[83] Y. Kawai, K. Mori, M. Kishimoto, K. Ishikura, and T. Shimada, "Surface Tension of Liquid Fe-C-Si Alloys," *Tetsu-to-Hagane*, vol. 60, no. 1, pp. 29–37, 1974, doi: 10.2355/tetsutohagane1955.60.1_29.

[84] V. M. Perevertailo, O. B. Loginova, and S. A. Lysovenko, "On the criteria for the surface activity and classification of the surface tension isotherms from the data on the melt structure," *J. Superhard Mater.*, vol. 37, no. 4, pp. 234–241, 2015, doi: 10.3103/S1063457615040036.

[85] C. Garcia-Cordovilla, E. Louis, and A. Pamies, “The surface tension of liquid pure aluminium and aluminium-magnesium alloy,” *J. Mater. Sci.*, vol. 21, no. 8, pp. 2787–2792, 1986, doi: 10.1007/BF00551490.

[86] L. M. Shergin, S. I. Popel’, and B. V. Tsarevsky, “Temperature dependence between densities and surface tension of cobalt–silicon and nickel–silicon melts,” *Phys. Chem. Metall. Melts*, vol. 25, p. 50, 1971.

[87] V. I. Nizhenko and Y. I. Smirnov, “Surface properties of manganese - TiN liquid alloys,” *Powder Metall. Met. Ceram.*, vol. 42, no. 9–10, pp. 517–522, 2003, doi: 10.1023/B:PMMC.0000013225.95000.c6.

[88] M. Kishimoto, K. Mori, and Y. Kawai, “Surface Tension of Liquid Fe－Ti and Fe-C-Ti Systems under H2 Atmosphere,” *J. Japan Inst. Met.*, vol. 48, pp. 413–417, 1984.

[89] B. V. T. L.A. Smirnov, S.I. Popel, “Izvestiya vysshikh uchebnykh zavedenii,” *Chern. Met.*, vol. 8, pp. 10–14, 1965.

[90] J. Lee, W. Shimoda, and T. Tanaka, “Surface tension and its temperature coefficient of liquid Sn-X (X=Ag, Cu) alloys,” *Mater. Trans.*, vol. 45, no. 9, pp. 2864–2870, 2004, doi: 10.2320/matertrans.45.2864.

[91] I. Seyhan and I. Egry, “Surface tension of undercooled binary iron and nickel alloys and the effect of oxygen on the surface tension of Fe and Ni,” *Int. J. Thermophys.*, vol. 20, no. 4, pp. 1017–1028, 1999, doi: 10.1023/A:1022638400507.

[92] A. Sharan and A. W. Cramb, “Surface tension and wettability studies of liquid Fe-Ni-O alloys,” *Metall. Mater. Trans. B*, vol. 28, no. 3, pp. 465–472, 1997, doi: 10.1007/s11663-

997-0113-4.

[93] I. Egry *et al.*, “Surface Tension, Phase Separation, and Solidification of Undercooled Cobalts-Copper Alloys,” *Adv. Eng. Mater.*, vol. 5, no. 11, pp. 819–823, 2003, doi: 10.1002/adem.200320508.

[94] P. Fima, “Surface tension and density of liquid Sn-Ag alloys,” *Appl. Surf. Sci.*, vol. 257, no. 8, pp. 3265–3268, 2011, doi: 10.1016/j.apsusc.2010.11.002.

[95] V. Krasovskyy and Y. Naidich, “Surface tension and specific volume of copper-titanium melts measured by the sessile drop method,” *J. Adhes. Sci. Technol.*, vol. 18, no. 4, pp. 465–471, 2004, doi: 10.1163/156856104323016360.

[96] S. Amore, J. Brillo, I. Egry, and R. Novakovic, “Surface tension of liquid Cu-Ti binary alloys measured by electromagnetic levitation and thermodynamic modelling,” *Appl. Surf. Sci.*, vol. 257, no. 17, pp. 7739–7745, 2011, doi: 10.1016/j.apsusc.2011.04.019.

[97] S. . Kaufman and T. . Whalen, “The surface tension of liquid gold, liquid tin, and liquid gold-tin binary solutions,” *Acta Metall.*, vol. 13, no. 7, pp. 797–805, Jul. 1965, doi: 10.1016/0001-6160(65)90144-6.

[98] X. J. Han, N. Wang, and B. Wei, “Thermophysical properties of undercooled liquid cobalt,” *Philos. Mag. Lett.*, vol. 82, no. 8, pp. 451–459, Aug. 2002, doi: 10.1080/09500830210144382.

[99] V. P. Krasovskyy, Y. V. Naidich, and N. A. Krasovskaya, “Surface tension and density of copper-zirconium alloys in contact with fluoride refractories,” *J. Mater. Sci.*, vol. 40, no. 9–10, pp. 2367–2369, 2005, doi: 10.1007/s10853-005-1960-5.

[100] E. Ricci *et al.*, "Surface tension and density of Si-Ge melts," *J. Chem. Phys.*, vol. 140, no. 21, 2014, doi: 10.1063/1.4879775.

[101] T. Ishikawa, P. F. Paradis, R. Fujii, Y. Saita, and S. Yoda, "Thermophysical property measurements of liquid and supercooled iridium by containerless methods," *Int. J. Thermophys.*, vol. 26, no. 3, pp. 893–904, 2005, doi: 10.1007/s10765-005-5585-3.

[102] O. Flint, "Surface tension of liquid metals," *J. Nucl. Mater.*, vol. 16, no. 3, pp. 16–260, Jul. 1965, doi: 10.1016/0022-3115(65)90113-3.

[103] K. Zhou, H. P. Wang, J. Chang, and B. Wei, "Experimental study of surface tension, specific heat and thermal diffusivity of liquid and solid titanium," *Chem. Phys. Lett.*, vol. 639, pp. 105–108, 2015, doi: 10.1016/j.cplett.2015.09.014.

[104] J. Tille and J. C. Kelly, "The surface tension of liquid titanium," *Br. J. Appl. Phys.*, vol. 14, no. 10, pp. 717–719, 1963, doi: 10.1088/0508-3443/14/10/332.

[105] T. Dubberstein, H. P. Heller, J. Klostermann, R. Schwarze, and J. Brillo, "Surface tension and density data for Fe–Cr–Mo, Fe–Cr–Ni, and Fe–Cr–Mn–Ni steels," *J. Mater. Sci.*, vol. 50, no. 22, pp. 7227–7237, 2015, doi: 10.1007/s10853-015-9277-5.

[106] J. Brillo, Y. Plevachuk, and I. Egry, "Surface tension of liquid Al-Cu-Ag ternary alloys," *J. Mater. Sci.*, vol. 45, no. 19, pp. 5150–5157, 2010, doi: 10.1007/s10853-010-4512-6.

[107] Z. Li, M. Zeze, and K. Mukai, "Surface Tension and Wettability of Liquid Fe-16mass%Cr-S Alloy with Alumina," *Mater. Trans.*, vol. 44, no. 10, pp. 2108–2113, 2003, doi: 10.2320/matertrans.44.2108.

[108] R. Nowak *et al.*, "Surface tension of γ-TiAl-based alloys," *J. Mater. Sci.*, vol. 45, no. 8,

pp. 1993–2001, 2010, doi: 10.1007/s10853-009-4061-z.

[109] R. Pajarre, P. Koukkari, T. Tanaka, and J. Lee, “Computing surface tensions of binary and ternary alloy systems with the Gibbsian method,” *Calphad*, vol. 30, no. 2, pp. 196–200, Jun. 2006, doi: 10.1016/j.calphad.2005.08.003.

[110] R. Aune *et al.*, “Surface tension and viscosity of industrial alloys from parabolic flight experiments - Results of the ThermoLab project,” *Microgravity Sci. Technol.*, vol. 15, no. 1, pp. 11–14, 2005, doi: 10.1007/bf02945937.

[111] T. Tanaka and S. Hara, “Thermodynamic evaluation of surface tension of liquid metal-oxygen systems,” *Steel Res.*, vol. 72, no. 11–12, pp. 439–445, 2001, doi: 10.1002/srin.200100149.

[112] Z. Li, K. C. Mills, M. McLean, and K. Mukai, “Measurement of the density and surface tension of Ni-based superalloys in the liquid and mushy states,” *Metall. Mater. Trans. B Process Metall. Mater. Process. Sci.*, vol. 36, no. 2, pp. 247–254, 2005, doi: 10.1007/s11663-005-0026-z.

[113] B. Oleksiak, J. Łabaj, J. Wieczorek, A. Blacha-Grzechnik, and R. Burdzik, “Surface tension of Cu - Bi alloys and wettability in a liquid alloy - Refractory material - Gaseous phase system,” *Arch. Metall. Mater.*, vol. 59, no. 1, pp. 281–285, 2014, doi: 10.2478/amm-2014-0046.

[114] D. K. Duvenaud, “Automatic Model Construction with Gaussian Processes David,” 2014.

Appendix 1: References of surface tension values

Alloy	Ref	Method	Alloy	Ref	Method	Alloy	Ref	Method
Fe-Cr	[68], [69]	LD,SD	Ni-Al	[70], [71], [72]	EL,OD	Al-Li	[42]	MGBP
Fe-Cu	[70], [68]	EL, SD	Ni-Cr	[69], [73]	SD, SD*	Al-Ti	[74]	EL
Fe-Sn	[68]	LD	Ni-Sn	[68]	LD	Al-Cu	[75], [76]	--, SD
Fe-Al	[72]	EL, OD	Ni-Co	[73]	SD*	Al-Si	[77],[78]	EL, OD, SD
Fe-Co	[44]	SD	Ni-W	[73]	SD*	Al-Zn	[79], [80] by [27]	--
Fe-Mo	[44],[27]	SD	Ni-Cu	[68]	LD, SD	Au-Si	[81]	Large drop
Fe-W	[44]	SD	Ni-Mo	[44]	SD	Al-Au	[82]	EL
Fe-Si	[83]	SD, PD	Ni-Ge	[84]	--	Al-Mg	[85], [80] by [27]	MGBP,SD
Fe-Ge	Zamarev et al 1976 by [27]	--	Ni-Si	[86] by [27]	--	Mn-Sn	[87]	SD
Fe-Ti	[88], [89] by [27]	--	Zn-Li	[42]	MGBP	Sn-Cu	[90]	CD
Fe-Ni	[91], [69] , [92], [45], [44]	--,SD, SD, EL, SD	Cu-Co	[93]	EL	Sn-Ag	[94], [90]	SD, CD
Zr	[43], [101], [104]–[107]	--	Cu-Ge	[84]	--	Au-Ge	[81]	Large drop
Nb	[43], [101], [102]	--	Cu-Ti	[95], [96]	SD, EL	Au-Sn	[97]	SD
Co	[98]	OD+EL	Cu-Zr	[99]	Large drop	Si-Ge	[100]	PD
Ni	[98]	OD+EL	Ta	[59], [101]	PD	Sn-Ge	[84]	--
Ti	[43], [102]–[104]	--				Mn-Ge	[84]	--

(a)

Alloy	Ref	Method		Alloy	Ref	Method
Fe-Cr-Mn-Ni	[105]	MGBP, SD		Ni-Cu-Fe-Sn-Ge	[34]	EL
AISI 304 steel	[105]	MGBP, SD, EL		Fe-Cu-Mo	[66]	EL
Ni-Cu-Fe-Sn	[34]	EL		Fe-Ni-Cr	[69]	SD
Al-Cu-Ag	[106]	EL		Fe-Cr-S	[107]	SD
Ti-Al-Nb	[108]	EL		Fe-Cr-Mo	[105]	MGBP, SD
Ti-Al-Ta	[108]	PD, SD		Fe-C-Si	[83]	SD
Ag-Au-Cu	[109]	SD		Ni-Cu-Fe	[34]	EL
Ti-Al-V	[110]	PF		Fe-Cr-Ni-S	[107]	SD

(b)

Alloy	Ref	Method		Alloy	Ref	Method		Alloy	Ref	Method
Bi-Sn	[79]	SD		Se-Na	[42]	MGBP		In-Na	[42]	MGBP
Bi-Pb	[79]	SD		Bi-Na	[42]	MGBP		Cs-Sb	[79]	SD
In-K	[42]	MGBP		Bi-K	[42]	MGBP		Pb-Sn	[79]	SD
Cs-Na	[42]	MGBP		Pb-Li	[42]	MGBP		In-Li	[42]	MGBP
Co-O	[111]	--		Fe-O	[111]	--		Ni superalloy CMSX-4	[40], [112]	SD, SD+
Cu-O	[111]	--		Ni-O	[111]	--		Ni superalloy CMSX-10	[112]	SD+
Fe-O-N	[18]	SD		Cu-Bi	[113]	--		Ni-alloy MM247LC	[110]	PF

(c)

Table A1 Complete database for development of the ML-GPR model. Systems and bibliographic references. (c) includes systems that were not taken into consideration. The abbreviations describe the experimental method used by the authors: SD= Sessile Drop, SD= improved SD, SD+= modified SD, CSD=Constrained SD, PF=Parabolic Flight, PD= Pendant Drop, MGBP=Maximum Gas Bubble Pressure, EL= Electromagnetic Levitation, OD= Oscillating Drop technique*

Appendix 2: Machine learning model and evaluation tools

Gaussian Process Regression [46], [57] (GPR, also known as Kriging, Gaussian spatial modeling, Gaussian stochastic process) is a method that can be used to model a complex relationship between an output and several inputs that cannot reasonably be approached by a simple linear model. GPR works by defining a distribution over functions and inference takes place directly in the space of functions. This gives an advantage over other non-statistical machine learning methods in that, in addition to predicting a mean value, it also provides a variance, or an error range, for the prediction distribution.

To explain the main mathematical principles behind Gaussian processes, let us consider a database D made of N measurements of a property (output) y, as a function of L variables (inputs), x^m as m varies from 1 to L. The input data $[X_N]$ can then be defined as an N L-dimensional input line vectors with: $[X_N]= \{ \vec{x}_1 , \vec{x}_2, \dots , \vec{x}_N \}$. The output column vector is $\vec{y}_M=\{ y_1 , y_2, \dots , y_N\}$.

Now, to predict an output y_{N+1} for a new input vector $\vec{x}_{N+1}$, the Gaussian process (GP) assumes that the joint probability distribution of the new point and the N points in the database D, $P(y_{N+1} | \vec{x}_{N+1} , D)$ is a multivariate Gaussian:

$$P(y_{N+1} \mid \vec{x}_{N+1} , D) = \frac{1}{\sqrt{2\pi}\sigma_{\hat{y}}} \exp[-\frac{(y_{N+1} - \hat{y})^2}{2\sigma_{\hat{y}}^2}]$$

where $\hat{y}$ and $\sigma_{\hat{y}}^2$ are its corresponding mean and standard deviation respectively. Statistically, the mean gives the most probable value of the output, predicted for the new set of inputs, and starting from known information contained in the database. With this being said, $\hat{y}$ is therefore the value we want to predict and $\sigma_{\hat{y}}$ provides an estimate of a predictive error. $\hat{y}$ is defined as:

$$\hat{y} = \vec{k}^T [C_N]^{-1} \vec{y}_N$$

where $\vec{k}$ is a column vector defined as:

$$\vec{k} = [\, C(\vec{x}_1, \vec{x}_{N+1}), C(\vec{x}_2, \vec{x}_{N+1}), \dots, C(\vec{x}_N, \vec{x}_{N+1})]$$

where $[C_N]$ is the covariance matrix which is a function of $[X_N]$. The elements of the covariance matrix, $C(\vec{x}_i, \vec{x}_j)$, are defined by the covariance function. This function defines how strongly any input can impact the value of the output. There exist several forms for this function. In the present case, the radial-basis function (RBF), also known as squared-exponential, is used and can be defined as follows:

$$C(\vec{x}_i, \vec{x}_j) = \theta . exp\left[-\frac{1}{2}\sum_{l=1}^{L}\frac{\left(x_i^l - x_j^l\right)^2}{r_l^2}\right] + \omega$$

Where θ , ω (not detailed here) and r_l are a set of parameters referred to as hyper-parameters, and are usually unknown and need to be inferred and optimized from the data during the learning process. Note that the covariance function gives the covariance between two outputs y_i and y_j and is written as a function of their corresponding inputs $\vec{x}_i$ and $\vec{x}_j$ (x_i^l and x_j^l being the corresponding coordinates in the l^{th} dimension). r_l is the lengthscale which specifies the width of the kernel in the l^{th} dimension and therefore the smoothness of its corresponding functions [114].

In fact, to get the best performance out of any selected machine learning model, tuning of the hyper-parameters (searching the hyper-parameter space for the best cross-validation results for the model) is needed. The most common method to achieve this is by applying a Gridsearch: constructing a grid containing the parameters one wishes to optimize. Usually, any parameter used to construct an estimator can be optimized in this manner. This works by defining a dictionary, a list of the parameters as well as a range for search. Each time, the model will be trained on a combination of these parameters and the results are finally compared to choose the best model, i.e.

the one with the highest prediction accuracy. Of course, this method is not optimal as the obtained optimal combination of parameters still depend on the manually set ranges of search. The effect of this issue can be lessened by simply increasing the number of values to be evaluated. Bearing in mind that this will significantly increase the computational time, a compromise must be made. Finally, the parameters are adjusted as to obtain the best possible description of data.

Additionally, even if the Bayesian nature of GPs normally automatically avoids overfitting, it is nevertheless preferable to check the predictive capacity of the model using cross-validation. One way to do this is using the K-fold cross validation method, described later on.

K-fold Cross Validation

One of the standard and commonly used methods for estimating the performance of a machine learning model is the K-fold cross validation. The dataset is divided into K folds, and a procedure is repeated K times, with the model being trained on K-1 folds and tested on the remaining fold. Calculating the accuracy of prediction in each procedure gives and evaluation of the predictability of the model and identification of its weak points. This method allows to evaluate different models and to compare them. During the K repeated trainings, the values of errors and evaluation metrics such as the Mean Squared Error (MSE), Mean Absolute Error (MAE) and R-Squared (R2) (equations are defined below) recorded and finally averaged for a global view. The predicted values are also recorded for a better visualization of the prediction compared to the real values.

Evaluation metrics

- Mean Squared Error (MSE):

$$MSE = \frac{1}{n}\sum_{i}(y - \hat{y})^2$$

- Root Mean Squared Error (RMSE): which is the square root of the MSE

- Mean Absolute Error:

$$MAE = \frac{1}{n}\sum_{i} |y - \hat{y}|$$

- R-squared (R^2):

$$R^2 = 1 - \frac{\sum_i (y - \bar{y})^2}{\sum_i (y - \hat{y})^2}$$

where y is the actual experimental value, $\bar{y}$ is the corresponding mean value and $\hat{y}$ is the predicted one, while i denotes the i-th data point among n.

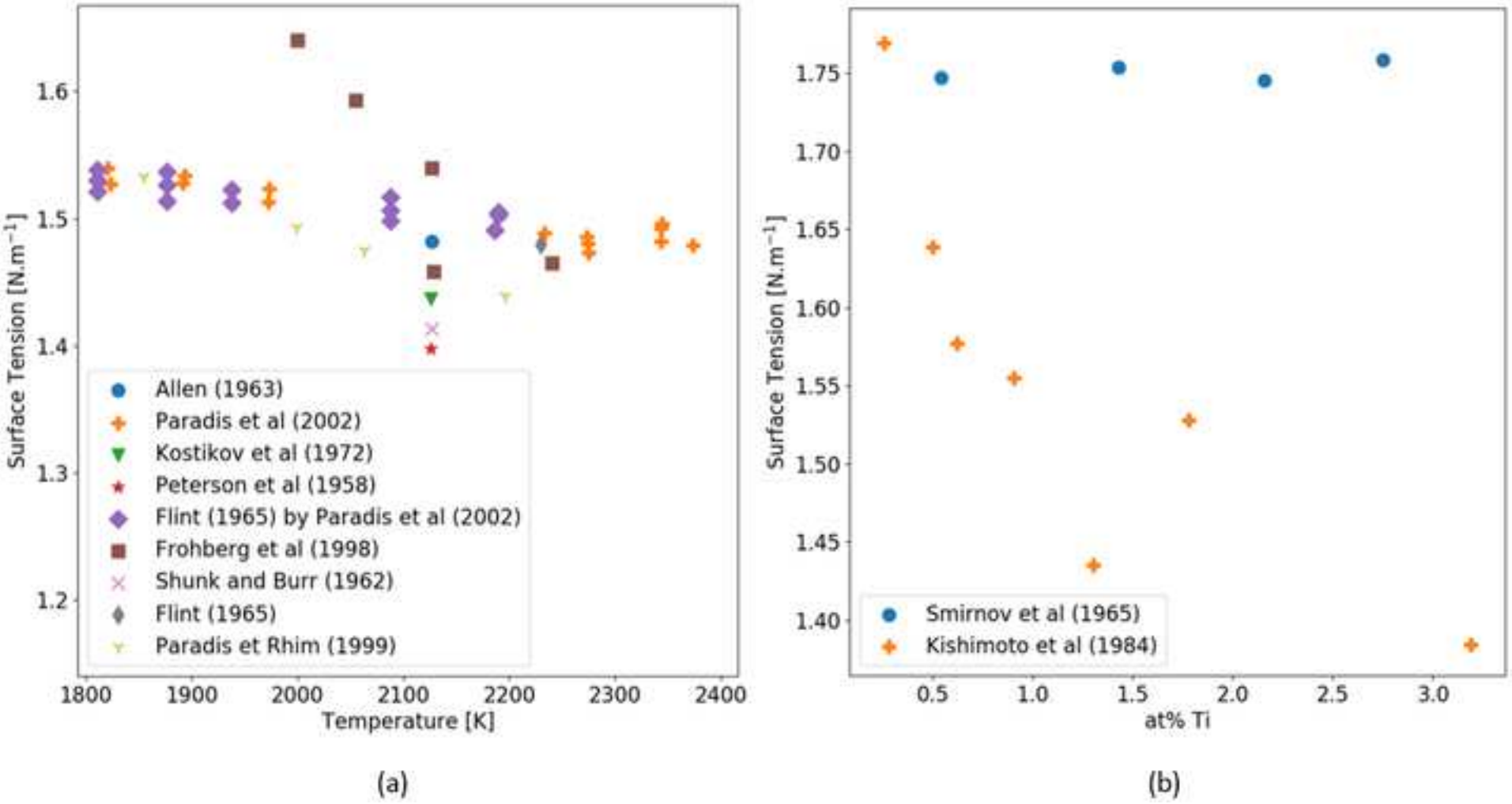

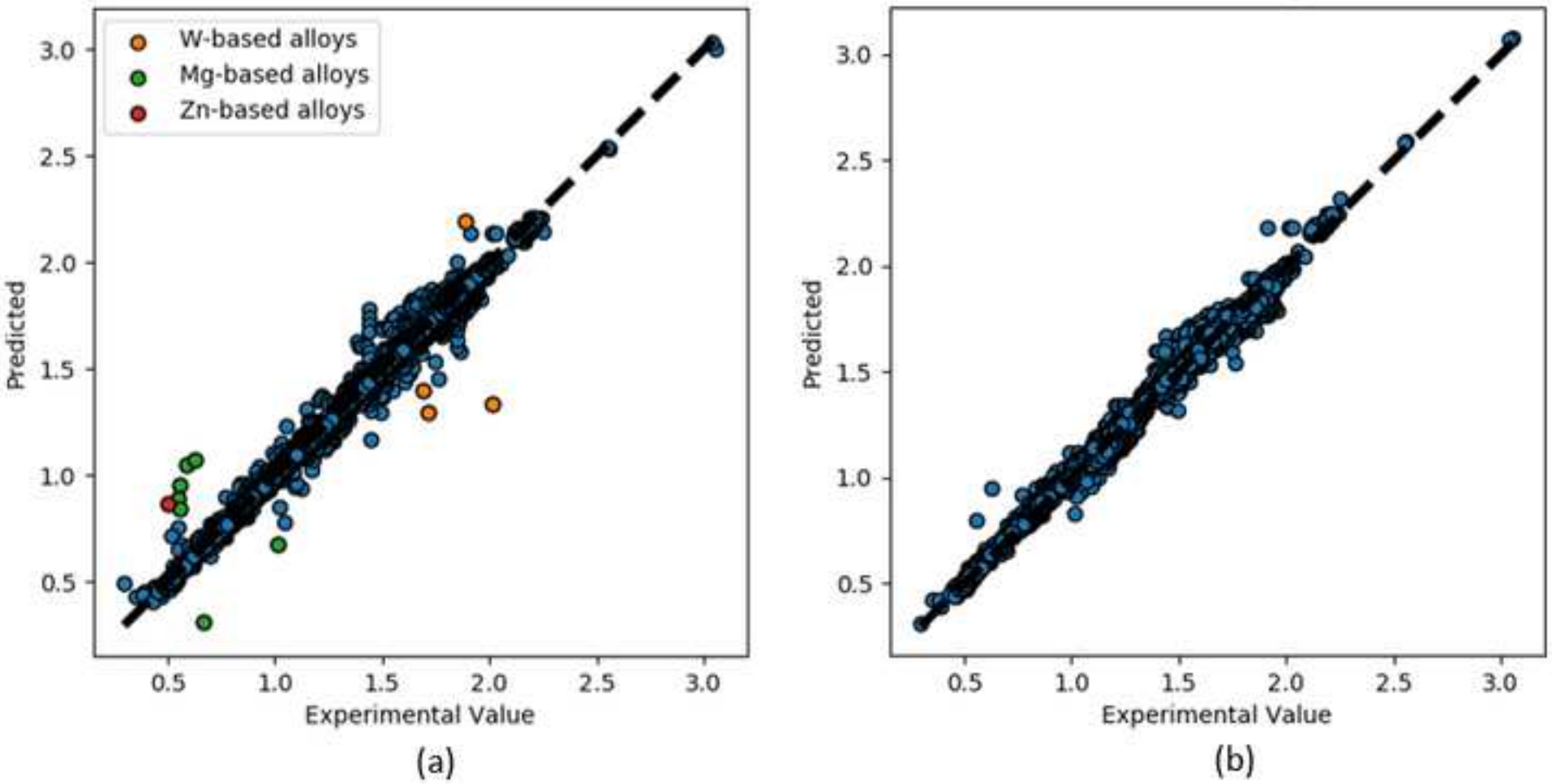

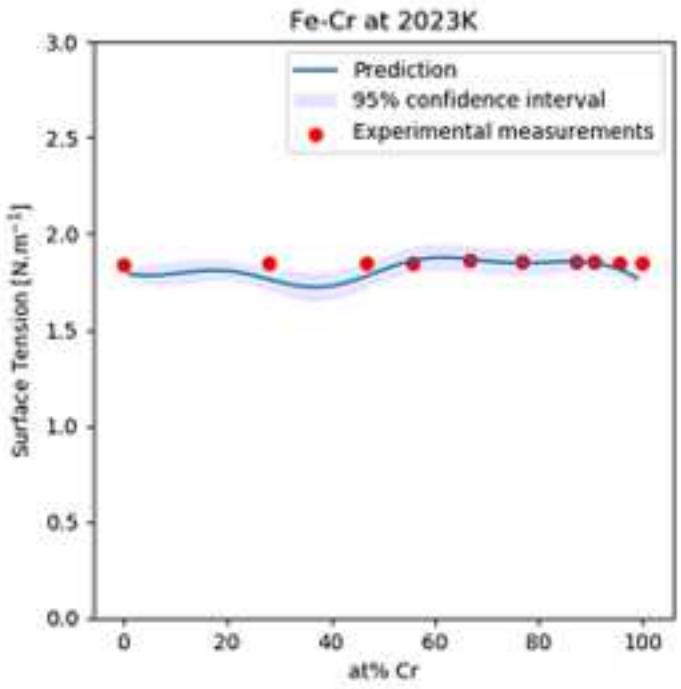

(a)

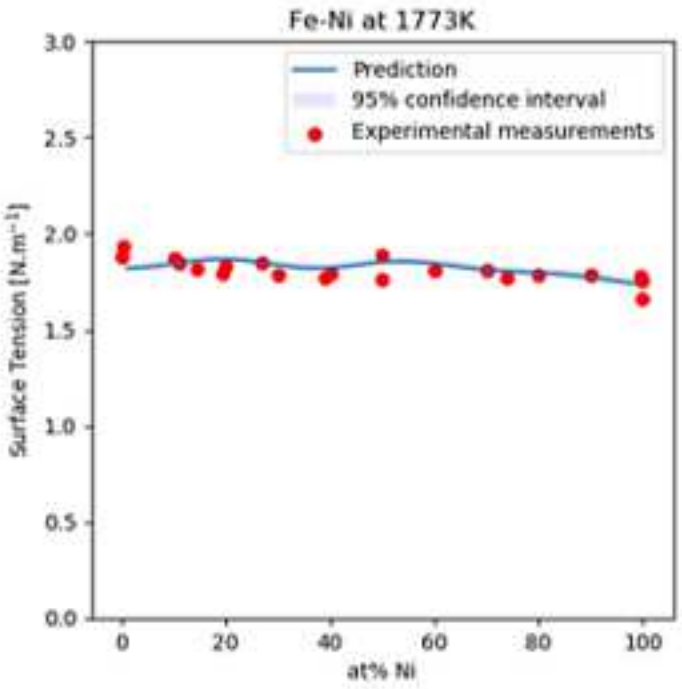

(b)

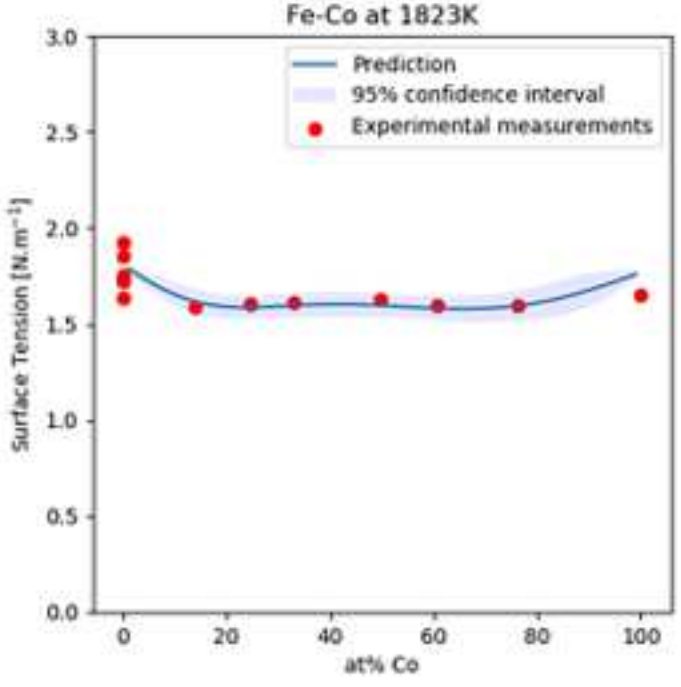

(c)

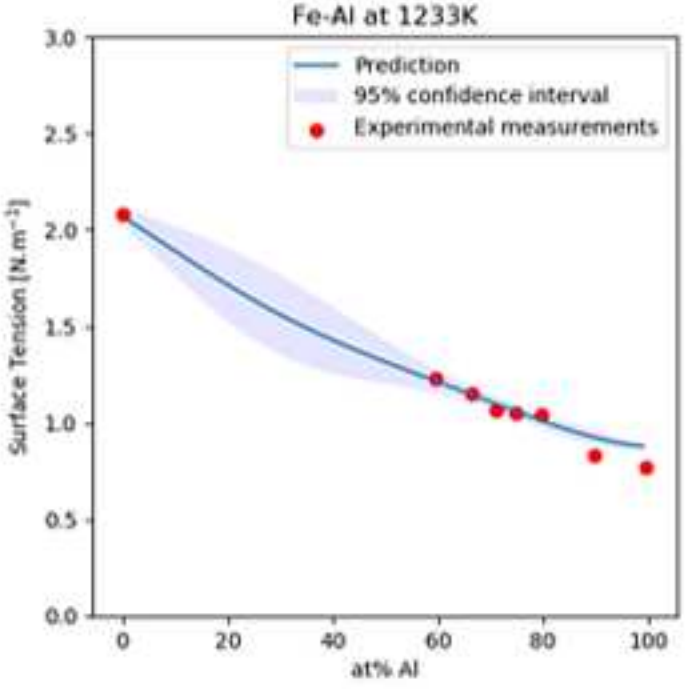

(d)